CONTROLS AND DYNAMICS OF SOLUTE TRANSPORT IN FLORIDA'S SPRING-FED KARST RIVERS

By

ROBERT HENSLEY

A THESIS PRESENTED TO THE GRADUATE SCHOOL
OF THE UNIVERSITY OF FLORIDA IN PARTIAL FULFILLMENT
OF THE REQUIREMENTS FOR THE DEGREE OF
MASTER OF SCIENCE

UNIVERSITY OF FLORIDA

2010

To my family and friends

ACKNOWLEDGMENTS

I thank my advisor Dr. Matt Cohen and the members of my committee, Dr. Tom Frazer and Dr. Jon Martin for offering their insight and advice. I thank Larry Korhnak and Chad Foster for assisting me in performing field work. I thank my wife and my parents for their support and encouragement.

TABLE OF CONTENTS

page

LIST OF TABLES

LIST OF FIGURES

LIST OF ABBREVIATIONS

A	Channel cross-sectional area (L^2)
A_H	Sediment cross-sectional area (L^2)
A_S	ADS model storage zone cross-sectional area (L^2)
A_V	Vegetation cross-sectional area (L^2)
α	ADS model storage zone exchange coefficient (1/T)
b	DHG width equation exponent
C	Channel solute concentration (M/L^3)
C_S	Storage zone solute concentration (M/L^3)
c_n	DHG equation coefficient
D	Dispersion coefficient (L^2/T)
D_z	Vertical diffusion (L^2/T)
Δt	Incremental time (T)
Δw	Incremental width (L)
Δx	Incremental distance (L)
f	DHG depth equation coefficient
h	Depth (L)
K	Hydraulic conductivity (L/T)
L	Reach length (L)
l	Sediment thickness
M_0	Zeroth moment (M)
M_1	First moment (MT)
M_{2Cent}	Centralized second moment (MT^2)
m	DHG velocity equation coefficient

P	Wetted perimeter (L)
Pe	Peclet number
Q	Flowrate (L^3/T)
R	Hydraulic radius (L)
σ^2	Temporal variance (T^2)
σ_θ^2	Dimensionless variance
σ_x^2	Spacial variance (L^2)
τ	Mean residence time (T)
u	Mean velocity (L/T)
u*	Shear velocity (L/T)
W	Mean Channel width (L)

Abstract of Thesis Presented to the Graduate School
of the University of Florida in Partial Fulfillment of the
Requirements for the Degree of Master of Science

CONTROLS AND DYNAMICS OF SOLUTE TRANSPORT IN FLORIDA'S SPRING-FED KARST RIVERS

By

Robert Hensley

August 2010

Chair: Name Matt Cohen
Major: Forest Resources and Conservation

As anthropogenic activities increasingly alter nutrient and hydrologic cycles, the role of river systems as both conduits and sinks for these nutrients has become ever more apparent. If we are to predict the transport and fates of these solutes, as well as their ecological implications, we must first understand the basic mechanism controlling the solute transport properties of river systems. Because of their point source nature, Florida's spring-fed rivers make ideal model ecosystems for studying solute transport. Despite having a long history of ecological study, to date no serious attempts have been made to determine the solute transport properties of these rivers, which act as one of the bottom-up control on the ecosystem structure and function.

The geomorphic and vegetative characteristics of nine spring-fed rivers were measured, which in many cases had never before been determined. These geomorphic and vegetative characteristics varied widely across rivers and also between reaches within rivers. The channel geometry and discharge relationships for the upstream reaches were markedly different from the downstream reaches, indicating different processes may be driving channel evolution.

A tracer tests using Rhodamine WT was used to determine the mean residence time as well as the solute transport properties by using a one dimensional advection dispersion and storage model to fit the breakthrough curve. In many cases even a two storage zone model failed to fit the long tails of the breakthrough curves, indicating that the residence times in these systems may follow a power law distribution, with some particles spending substantially longer than the mean residence time in the system. The mean velocity and therefore the mean residence time was found to be negatively correlated with the percentage of the channel cross-section obstructed by vegetation. The magnitude of dispersion was determined to be most dependent of the velocity, with a greater velocity producing more shear stress and greater dispersion. The magnitude of transient storage was determined to be a function of both the vegetation storage and hyporheic storage.

Results indicate that maximizing vegetation is ideal if managing for maximum nutrient removal. In addition to direct effects (assimilation) and first-order indirect effects (by providing the carbon which drives processes such as denitrification), vegetation also exerts second-order indirect effects on nutrient cycling by extending the residence time so that more assimilation and denitrification may occur.

Understanding the geomorphic and vegetative characteristics which control the solute transport properties of these systems is an important early step in the ongoing process of determining these mechanisms in a more general sense for large rivers everywhere, and their role in controlling the transport and fate of dissolved nutrients.

CHAPTER 1
INTRODUCTION

Importance of Understanding River Hydraulics

In lotic systems, channel hydraulics control nutrient flux and hydraulic residence times, which act as bottom-up controls on ecological processes such as biogeochemical processing. As anthropogenic modification of nutrient and hydrologic cycles has intensified (Vitousek et al. 1997), the importance of stream and river networks as sinks for contaminants has become increasingly apparent. In particular, the hydraulic properties of lotic systems appear to control nitrogen processing (Seitzinger et al. 2002, Ensign et al. 2006, Alexander et al. 2009), though large uncertainties remain about such processing in large (> 10 m^3/s) rivers because most studies have focused on small streams (Ensign et al. 2006, Tank et al. 2008). A clear need exists to understand solute transport and reactivity in large rivers, and a precondition for addressing contaminant fate and transport is detailed information about the factors controlling river hydraulics.

Numerous previous studied have attempted to quantify the geomorphic and vegetative controls on solute transport, however the majority of these studies have consisted of small scale flume tests (Nepf et al. 1997, Nepf 1999, Carollo et al. 2002, Wilson et al. 2002, Wilson et al. 2003, Carollo et al. 2005, Jarvela 2005, Murphy et al. 2007, Wilson 2007, Shucksmith et al. 2010), and studies conducted on natural streams have primarily focused on smaller streams (Ensign et al. 2006, Tank et al. 2008) such as pool and riffle mountain stream (Day 1975, Bencala et al. 1983a, Bencala et al. 1983b, Bencala et al. 1984). Only recently have studies been performed on larger rivers with channel widths on the scale of tens of meters and reach lengths on the scale of several kilometers

North Florida is world renowned for its abundance of artesian spring fed rivers. It features the highest density of springs anywhere in the world, with over thirty 1st order (>2.8 m^3/s mean discharge) springs, and over 700 named springs (Scott et al. 2004). These ecosystems are incredibly productive and support a rich biodiversity. Apart from their ecological value, there are several properties of these rivers which make them ideal model ecosystems for studying nutrient cycling as well as ecosystem metabolism, with implications for large rivers elsewhere. Because of the point source nature of nearly all the discharge emanating from a spring vent, the inputs to the system are easy to quantify. Additionally, the discharge, water temperature, and water chemistry remain nearly constant from season to season (Odum 1957a, Odum 1957b). These properties make spring-fed rivers the closest approximation to chemostats as can be observed in nature. However, despite their long history of ecological study, to date no serious attempts have been made to measure the hydraulic properties of these rivers. While several studies have measured the geomorphic and vegetative properties of these rivers (Kurtz et al. 2003, Hoyer et al. 2004), to my knowledge none have attempted to quantify the effects of these properties on river hydraulics.

Advection

Determining the hydraulic properties of a river such as mean velocity and retention time is essential in understanding ecological processes such as nutrient transport and metabolism. This is because solutes such as nutrients which are dissolved in a fluid are carried along by that fluid as it travels; this principle is known as advection.

The mean velocity of a fluid traveling through an open channel is a function of the channel geometry, channel roughness and channel slope (Manning 1890, Manning 1895, Chow 1959). This relationship has been understood for over 100 years and is

described by Manning's equation, an empirical equation containing the coefficient n. This Manning coefficient is essentially a correction factor due to the loss of energy through friction at the fluid-substrate interface, and is a function of properties of the river, including substrate roughness, variation in channel cross sectional area, substrate sediment type, channel irregularities and constrictions, obstructions such as vegetation, and sinuosity (Chow 1959). Numerous studies have utilized flume tests to determine the effects of vegetation on Manning coefficients, both empirically based, such as the n-uR method (Palmer 1945, Ree 1949), and also based on the bio-mechanical properties of the vegetation itself (Kouwen et al. 1969). The general conclusion of these studies is that as density of vegetation in the channel increases, the Manning coefficient also increases, which would correspond with a decrease in mean velocity.

While it is a well accepted and excellent tool for estimating properties such as river stage, one of the major shortcoming of using Manning's equation (and many other similar equations such as the Bernoulli or Chezy equation), is that they can only predict the mean velocity (and therefore residence time) and not the velocity distribution. In the case of ideal plug flow, water moves as a continuous slug, and particles released at an upstream boundary would arrive at the downstream boundary simultaneously. The breakthrough curve for ideal plug flow would resemble a Dirac delta function, with a concentration of zero at all times other than the mean residence time. Plug flow is almost never observed in reality however. Actual breakthrough curves usually resemble a skewed Gaussian function with a center of mass located at the mean residence time. This indicates a distribution of velocities caused by a longitudinal spreading of the particles.

Dispersion

The dispersion coefficient (D) describes this longitudinal spreading. The dispersion coefficient is equal to one half the rate of change in longitudinal variance in particle distribution (σ_x^2) (Murphy et al. 2007).

$$D = \frac{1}{2}\frac{d\sigma_x^2}{dt} \quad (1\text{-}1)$$

There are a number of different mechanisms which cause dispersion. The resistance to flow due to friction at the fluid-substrate interface creates shear stress. This shear stress results in non-uniform vertical velocity profile (Taylor 1954, Elder 1959). The result of water near the surface moving faster than the water near the substrate interface is a separation of the flow known as vertical shear stress dispersion.

In addition to vertical shear stress dispersion, the presence of obstructions such as vegetation within the flow path can create additional dispersion. Because of shear stress, water traveling between obstructions is traveling faster than the water adjacent to the obstructions, resulting in a non-uniform lateral velocity profile (Lightbody et al. 2006). Vegetation heterogeneity will amplify this effect. Obstructions also alter the lateral velocity profile by creating turbulence. The magnitude of this turbulence is a function of the stem diameter of the obstruction and the Reynolds number, which is a ratio of the inertial forces to the viscous forces acting on an object submerged in a moving fluid. At intermediate Reynolds numbers, recirculation vortices can form behind obstructions, and transport in and out of these zones is through diffusion only. This concept will be discussed later as a possible mechanism for creating transient storage zones within the river system (Nepf et al. 1997). Additionally, because flowpaths around multiple obstructions are often circuitous, and two particles which begin side by

side may take drastically different times to travel the same longitudinal distance (Nepf et al. 1997, Nepf 1999). This process is known as mechanical dispersion.

The vertical shear stress dispersion, lateral shear stress dispersion and mechanical dispersion due to vegetation can be combined numerically into a single longitudinal dispersion coefficient (D). The advective and dispersive components of the flow can be combined into a transport equation which describes the change in concentration (C) of a conserved dissolved solute over time (Fischer 1973).

$$\frac{\partial C}{\partial t} = -u\frac{\partial C}{\partial x} + D\frac{\partial^2 C}{\partial x^2} \qquad (1\text{-}2)$$

Transient Storage Zones

While a transport equation which incorporates dispersive forces in addition to advection will result in a residence time distribution, an additional transient storage component is most often required to account for the pronounced 'tail' of a tracer breakthrough curve (Bencala et al. 1983a). Transient storage zones are locations within or adjacent to the channel in which the flow is stagnant relative to the advective flow, and may include dense vegetation beds, hyporheic zones, side pools and riparian wetlands (Bencala et al.1983, Choi et al 2000). As discussed above, vegetation and other channel obstructions are capable of creating transient storage zones (Nepf et al. 1997). Often, a near stagnant velocity can be observed within dense vegetation beds (Sand-Jensen et al. 1996), but an accelerated flow above the bed. This effect has been observed in the aquatic grass beds common in Florida's spring-fed rivers (Odum 1957a).

Another example of a possible transient storage zone is the hyporheic zone (Bencala et al. 1984, Harvey et al. 1996). The hyporheic zone is the saturated

sediments underlying and adjacent to the stream. Because transport in and out of the pore water between saturated sediments is much slower than advective flow, hyporheic sediments act as transient storage zones. Multiple storage zones with different spatial and temporal characteristics can often coexist within the same river (Choi et al. 2000). One type of storage zone may be much larger than another, but at the same time the exchange rate with the advective channel may be smaller, creating a complex solute transport system.

Advection, Dispersion and Storage Equation

The advective, dispersive and transient storage components can be combined to form the one dimensional advection dispersion and storage equation (ADS). This equation relates the change in solute concentration with respect to time at a given location to the sum of three components: advection, dispersion and storage (Bencala et al. 1983a, Bencala et al. 1990, S.S.W. 1990, Runkle 2007).

$$\frac{\partial C}{\partial t} = -u\frac{\partial C}{\partial x} + D\frac{\partial^2 C}{\partial x^2} + \alpha(C_S - C) \qquad (1\text{-}3)$$

The advective component is equal to the negative velocity times the longitudinal concentration gradient. The negative signs accounts for the fact that when there is a positive concentration gradient (i.e., lower concentration upstream than downstream), the concentration with respect to time will decrease, and vice versa. The dispersion component is equal to dispersion coefficient (D) times the second derivative (or longitudinal rate of change) of the longitudinal concentration gradient. The transient storage component is equal to the exchange coefficient (α) times the difference in concentration between the storage zone and the channel. In addition, because of this

channel-storage exchange, the concentration in the storage zone also changes with respect to time.

$$\frac{\partial C_S}{\partial t} = \alpha \frac{A}{A_S}(C - C_S) \quad (1\text{-}4)$$

The rate of change of the storage zone concentration (C_s) with respect to time is equal to the exchange coefficient (α) times the ratio of the channel cross sectional area (A) to the storage zone cross sectional area (A_s), times concentration gradient between the channel and the storage zone. Note that concentration gradient ($C\text{-}C_S$) in this equation is reverse to the one for the channel equation. This accounts for the fact that when there is a higher concentration in the channel than the storage zone, the concentration in the storage zone will increase, while the channel concentration will decrease, and vice versa.

There are some limitations to the one dimensional advection dispersion and storage equation. Foremost, it is a partial differential equation and requires a finite difference estimation to solve (Runkle 1998). Secondly, it is unidirectional, while in reality forces such as dispersion act in all three directions. Another is that in most previous applied cases, the equation only contains a single storage zone while in reality multiple transient storage zones exist (Choi et al. 2000). Finally, the model coefficients, such as channel cross sectional area, storage cross sectional area and exchange rates are constants, while in reality they are probably spatially variable. How to compensate for these limitations will be discussed in the methods section.

Hypothesis

From both the classical velocity prediction equations (Mannings Equation) and the ADS equation it is apparent that geomorphic and vegetative characteristics affect the

transport of dissolved solutes. Channel cross-sectional area, the dispersion coefficient, the storage zone cross sectional area and the storage zone exchange coefficient are all variables in the transport equation and would affect modeled transport of dissolved solutes, and these parameters are, in turn, controlled by the morphology of the channel, the density and cover of vegetation, the abundance of coarse woody debris and the properties of the channel sediments.

- The channel geometry of river systems is not random, but is dependent primarily on the discharge (Leopold et al. 1953, Leopold et al. 1964, Park 1977). It is expected that these same relationships between mean width, mean depth and discharge will be observed in these rivers as well.

- Channel geometry acts as a control on the magnitude of dispersion. Shear stress separation due to friction between the water and the benthic surface is a significant cause of dispersion (Taylor 1954, Elder 1959). As the hydraulic radius (normalized for discharge) decreases, a greater fraction of the flow will be in contact with the bed surface, increasing the shear stress and the magnitude of dispersion. As the channel area (normalized for discharge) decreases, a greater fraction of the flow will also be in contact with the bed surface and the same effects of shear stress on dispersion should be observed. Additionally, both Manning's equation and the continuity equation state that channel area is a major factor determining the mean velocity. As the mean velocity increases, the uniformity in the vertical velocity profile will decrease and the magnitude of dispersion will increase. It is therefore expected that the dispersion coefficient obtained from the ADS model will correlate with both the normalized hydraulic radius and the mean velocity.

- Vegetation also controls the magnitude of dispersion. Numerous flume studies have shown that vegetation creates dispersion by creating turbulence and a non-uniform later velocity profile (Nepf et al. 1997, Nepf et al. 1999, Lightbody 2006). This principle should be observed in natural rivers as well, and therefore the dispersion coefficient obtained from the ADS model is expected to correlate with the measured vegetation density.

- Vegetation controls the magnitude of transient storage. At least two transient storage zones are likely to exist in these rivers; dense vegetation beds and the underlying sediments. While the sediment cross sectional area is expected to be significant, the hydraulic conductivities of these sediments are expected to be low. For this reason, the total storage zone cross sectional area obtained from the ADS model is expected to correlate most closely with the measured vegetation cross-sectional area.

CHAPTER 2
METHODS

Site Descriptions

Nine spring-fed rivers in north central Florida were chosen for the study. The sites were chosen because they exhibit varying morphological and vegetative characteristics, varying by over an order of magnitude in discharge, an order of magnitude in mean width, and from almost totally vegetated to completely bare. Accessibility and permitting issues were also taken into account in site selection as two are located in a national forest, five are located in state parks, and one is located on private land where the owner graciously granted permission to perform the study. The study sites were: Alexander Creek, Blue Spring, Ichetucknee River, Juniper Creek, Mill Pond Spring, Rainbow River, Rock Springs Run, Silver River, and Weeki Wachee River (Figure 2.1). For the tracer study, each river was partitioned into two reaches with the boundaries of these reaches chosen based on morphological or vegetative differences observed during river characterization. The tracer release occurred at the upstream end of the upstream reach, and tracer monitoring stations were located at the downstream end of each reach.

Alexander Creek is located in Lake County Florida in the Ocala National Forest. The upstream reach began approximately 100 meters downstream of the main spring vent, adjacent to the canoe launch area. The total upstream reach length was 1,300 meters long. The total downstream reach was 1,800 meters long, ending approximately 1,200 meters downstream of the Country Road 445 bridge. Morphologic and vegetative characteristics for Alexander Creek were obtained from a total of eight transects, four in the upstream reach and four in the downstream reach (Figure 2-2a).

Blue Spring is located in Gilchrist County Florida, on the south side of the Santa Fe River. The upstream reach began just downstream of the main spring vent, adjacent to the swimming platform. The upstream reach was 140 meters long, ending just downstream of the canoe launch platform. The downstream reach was 210 meters long, ending just before the confluence with the Santa Fe River. Morphologic and vegetative characteristic for Blue Spring were obtained from a total of three transects, one in the upstream reach and two in the downstream reach (Figure 2-2b).

The Ichetucknee River is located in Columbia County Florida in the Ichetucknee Springs State Park. It is formed by the combined discharge of six major and numerous more minor springs. The upstream reach began approximately 600 meters downstream of the main spring vent, just downstream of the confluence with Blue Hole and adjacent to Trestle Point. The upstream reach was 1,800 meters long, ending at the Midway dock. The downstream reach was 2,500 meters long, ending at the South Takeout dock just upstream of the US Highway 27 Bridge. Morphologic and vegetative characteristic for the Ichetucknee River were obtained from a total of ten transects, five in the upstream reach and five in the downstream reach (Figure 2-2c).

Juniper Creek is located in Lake County Florida in the Ocala National Forest. The upstream reach began approximately 200 meters downstream of the main spring vent, at the confluence with Fern Hammock Spring. The upstream reach was 1,700 meters long. The downstream reach was 1,000 meters long. Morphologic and vegetative characteristic for Juniper Creek were obtained from a total of ten transects, five in the upstream reach and five in the downstream reach (Figure 2-2d).

Mill Pond Spring is located in Columbia County Florida, and is one of the six major springs that contribute to the Ichetucknee River (Figure 2-2c). Because of its short length, only a single reach was used. The reach began at the main spring vent and was 160 meters long, ending at the confluence with the Ichetucknee River. Morphologic and vegetative characteristic for Mill Pond were obtained from a total of seven transects.

The Rainbow River is located in Marion County Florida. The upstream reach began approximately 500 meters downstream of the main spring vent, at the boundary of Rainbow Springs State Park. The upstream reach was 1,800 meters long, ending just downstream of K.P. Hole Park. The downstream reach was 2,500 meters long, ending approximately 1,300 meters upstream of the County Road 484 Bridge. Morphologic and vegetative characteristic for the Rainbow River were obtained from a total of eight transects, four in the upstream reach and four in the downstream reach (Figure 2-2).

Rock Springs Run is located in Orange County Florida. The upstream reach began approximately 1,300 meters downstream of the main spring vent, at the third landing of Kelley Park. The upstream reach was 700 meters long, and the downstream reach was 2,300 meters long. Morphologic and vegetative characteristic for the Rock Springs Run were obtained from a total of seven transects, three in the upstream reach and four in the downstream reach (Figure 2-2).

The Silver River is located in Marion County Florida. The upstream reach began approximately 1,300 meters downstream of the main spring vent, just upstream of the boundary of Silver River State Park. The upstream reach was 1,550 meters long, ending just upstream of the Silver River State Park canoe launch. The downstream

reach was 5,300 meters long, ending approximately 600 meters upstream of the confluence with the Oklawaha River. Morphologic and vegetative characteristic for the the Silver River were obtained from a total of nine transects, three in the upstream reach and six in the downstream reach (Figure 2-2).

The Weeki Wachee River is located in Hernando County Florida. The upstream reach began approximately 100 meters downstream of the main spring vent, adjacent to the water slide. The upstream reach was 1,300 meters long. The downstream reach was 2,000 meters long. Morphologic and vegetative characteristic for the Weeki Wachee River were obtained from a total of eight transects, four in the upstream reach and four in the downstream reach (Figure 2-2).

River Characterization

To calculate river discharge at the time of the tracer test, total water depth and velocity measurements (at 0.6*depth) were recorded at 2- to 3-m increments across the span of the river at or near the end of the downstream reach. Water depth was determined by measuring the distance from the benthic surface to the water surface. In shallower areas this was done using a meter stick, while in deeper areas it was done by dangling a weight from a tape measure. Velocity was measured using an acoustic Doppler velocity meter (Sontek, San Diego, CA). Discharge was calculated using the section method where discharge equals the sum of the products of depth (h), velocity (u) and the incremental width (Δw):

$$Q = \sum h_i u_i * \Delta w = (h_1 u_1 + h_2 u_2 \ldots . h_n u_n) * \Delta w \quad (2\text{-}1)$$

These calculated discharge values were compared to USGS monitoring gauge data when available. The calculated discharges were also later checked through mass recovery analysis during the tracer test, which will be discussed later.

To characterize river geomorphic and vegetative properties, additional transects were run across each river. The total number of transects per river ranged from three for smaller runs up to ten or more for the larger rivers. Along each of these transects, measurements of a variety of attributes were taken at two to three meter increments. First, water depth and stream width were measured as before. Second, the vegetation height was determined by measuring the distance from the benthic surface to the approximate top of the deflected vegetation. As with water depth, this was done using a meter stick in shallower areas, while it was done by dangling a weight from a tape measure in deeper areas. These measurements were used to calculate vegetative frontal area and plant bed volume.

From these data points a cross-sectional profile of the channel and vascular plant beds at each transect was created. In a manner similar to discharge, the total channel cross sectional area was calculated using the section method (Figure 2-3) where area (A) equals the sum of the product of depth (h) and the incremental width (Δw):

$$A = \sum h_i * \Delta w = (h_1 + h_2 \ldots . h_n) * \Delta w \qquad (2\text{-}2)$$

The cross sectional area of the vegetation beds (A_V) was calculated in the same way based on the depths of the plant beds. Channel depth data were also used to compute the wetted perimeter, which is the length of channel bed in contact with the flow. It was calculated using the Pythagorean Theorem using the equation below in

where wetted perimeter (P) equals the sum of the square roots of the change in depth squared plus the incremental width squared:

$$P = \sum \sqrt{(h_{i+1} - h_i)^2 + \Delta w^2} \quad (2\text{-}3)$$

The hydraulic radius at each transect was calculated by dividing channel cross sectional area by the wetted perimeter:

$$R = \frac{A}{P} \quad (2\text{-}4)$$

It is worth noting that due to the channel geometry of these rivers (an order of magnitude wider than deep), the wetted perimeter effectively converged on the surface width, and therefore the hydraulic radius effectively converged on the mean depth.

The sediment depths along each transect were determined by measuring the distance from the benthic surface to the underlying bedrock. This was done using a thin steel sediment probe with attachable extensions and a slide hammer. In some cases, the depth of sediment exceeded the length of the probe and all available extensions (several meters in depth). In these cases, the maximum depth penetrated was recorded. These data were used to calculate the underlying sediment cross sectional area (A_H) using the same method as above.

Finally, the hydraulic conductivity of the sediments was determined by performing a falling head slug test. This was done at two to three locations along each transect, usually in the center of the channel and halfway between the center of the channel and each bank. A two-inch diameter PVC well was used; the well was open on only the bottom and was inserted 10 cm into the benthic sediments. A high precision level logger (Solinst Gold, Georgetown, ON) was lowered into the well and the water level

was allowed to equalize for several minutes to determine the initial head (h_0). A displacement slug was then lowered into the well and the response curve was recorded over several minutes using a ten second sampling interval. The hydraulic conductivity was calculated using the equation below where the hydraulic conductivity (K) equals the natural log of head 1 (h_1) divided by head 2 (h_2) times the sediment thickness (l) divided by the time for the water level to drop from head 1 to head 2:

$$K = \ln\left(\frac{h_1}{h_2}\right)\frac{l}{t} \tag{2-5}$$

In this case, h_1 is a constant, the water surface elevation after the addition of the displacement slug. Head 2 is the water surface elevation after time t. By rewriting equation (2-5) and plotting the values with respect to time it is possible to determine K from the slope of the best fit line.

$$l * \ln\left(\frac{h_1}{h_2}\right) = Kt \tag{2-6}$$

Channel Geometry and Discharge Relationships

Numerous previous studies (Leopold et al. 1953, Leopold et al. 1964, Park 1977) have found that channel geometry is correlated with discharge. The relationship between mean channel width, mean depth (essentially the same as hydraulic radius), and mean velocity can be described by the downstream hydraulic geometry (DHG) equations:

$$W = c_1 Q^b \tag{2-7}$$

$$h = c_2 Q^f \tag{2-8}$$

$$u = c_3 Q^m \quad (2\text{-}9)$$

The coefficients and exponents which describe these relationships are determined by the properties of the river. The product of the coefficients ($c_1 * c_2 * c_3$) and sum of the exponents (b + f + m) should theoretically equal one because discharge is the product of width (W), depth (h) and velocity (u). These coefficients and exponents were determined for spring rivers as a whole, and also for the upstream and downstream reaches separately to determine if they have different values, indicating different discharge-channel geometry relationships. It is worth reiterating that the location of the break between the upstream and downstream reaches was selected based on changes in channel morphology. In nearly all cases these breaks were abrupt and distinct enough to be visually discernable.

Tracer Test and Breakthrough Curve

The tracer release consisted of a single pulse of Rhodamine WT (Keystone Aniline Corportation, Chicago, IL), a conservative dye that fluoresces at 580 nm under light at 550 nm. The total mass of tracer released was determined by targeting a downstream peak concentration of 20 µg/L based on historically measured discharge and expected dispersion over the combined upstream and downstream reach length. Tracer breakthrough was measured at the downstream end of each reach using a Turner Design (Sunnyvale, CA) C3 fluorometer. The fluorometers were calibrated using a two-point curve with 0 µg/L and 10 µg/L standards. The fluorometers were set to sample every minute, and were allowed to collect data until it was reasonable to assume all the tracer had been transported through the system. This varied from a few hours in smaller systems to a full day or more in larger rivers.

The first step in analyzing the breakthrough curve was to filter out any interference caused by dissolved organic matter (DOM). Because DOM may fluoresce at the same wavelength as Rhodamine WT, it can cause the fluorometer to overestimate tracer concentrations. To correct for this potential source of error, baseline readings of DOM (obtained with the same C3 fluorometer) and Rhodamine WT concentrations were taken before the tracer test. A simple linear regression was done to determine the relationship between the two. The parameters of that regression were used to subtract the overestimation of Rhodamine WT concentrations from the total during dye breakthrough.

Next, moment analysis was performed on each breakthrough curve. All of the following moment analysis equations come from Kadlec and Knight (1996) unless otherwise noted. The area under the breakthrough curve is known as the zeroth moment. To calculate the zeroth moment of the curve, the sum of the individual concentration readings is multiplied by the time step of one minute (Figure 2-4). This area under the curve value is in units of µg*min/L, and multiplying by the discharge in L/min results in the mass of tracer recovered in µg.

$$M_0 = Q\int_0^\infty C(t)dt = Q\sum C_i \Delta t = (C_1 + C_2 \ldots . C_n) * \Delta t \qquad (2\text{-}10)$$

Total mass recovery divided by the mass injected upstream yields a fractional mass recovery which is useful for verifying that the discharge value is correct and the fluorometers were properly calibrated. It also helps verify that any DOM interference was filtered out properly.

After the mass recovery was calculated from the zeroth moment of the breakthrough curve, the mean residence time was calculated using the first moment of

the curve. Each incremental area under the curve multiplied by its distance from the origin results in a value, the sum of which is known as the first moment. Dividing this first moment by the total area under the curve (the zeroth moment) yields the centroid of the curve, or the mean residence time. This centroid is the mean residence time (τ).

$$M_1 = Q\int_0^\infty C(t)tdt = Q\sum C_i t_i \Delta t = (C_1t_1 + C_2t_2 \ldots . C_nt_n) * \Delta t \quad (2\text{-}11)$$

$$\tau = \frac{M_1}{M_0} \quad (2\text{-}12)$$

The length (L) of each reach was determined by measuring the distance from the upstream boundary to downstream boundary along the center of the channel using aerial images. For the initial reach, the tracer release point served as the upstream boundary. The downstream boundary of this initial reach was then used as the upstream boundary of the subsequent reach. The mean velocity of each reach was calculated by dividing the reach length by the mean residence time.

$$u = \frac{L}{\tau} \quad (2\text{-}13)$$

The temporal variance (σ_t^2) of the breakthrough curve was then determined using the centralized second moment (centralized about the mean residence time). The temporal variance is a measure of the spread of the tracer, and is calculated by dividing the centralized second moment by the zeroth moment.

$$M_{2Cent} = Q\int_0^\infty C(t)(t-\tau)^2 dt = Q\sum C_i (t_i - \tau)^2 \Delta t = (C_1(t_1 - \tau)^2 \ldots . C_n(t_n - \tau)^2) * \Delta t \quad (2\text{-}14)$$

$$\sigma_t^{\,2} = \frac{M_{2Cent}}{M_0} \quad (2\text{-}15)$$

This temporal variance has units of time squared. The resulting value cannot be compared across different breakthrough curves because the magnitude of the variance is dependent on the time spent in the reach. To standardize the variance across systems and reaches, the variance is divided by the mean residence time squared. This new value is called the dimensionless (or normalized) variance (σ_θ^2). The dimensionless variance ranges from zero to one, with a value of zero representing absolute plug flow and a value approaching one representing maximum dispersion.

$$\sigma_\theta{}^2 = \frac{\sigma_t{}^2}{\tau^2} \tag{2-16}$$

$$0 \leq \sigma_\theta{}^2 \leq 1 \tag{2-17}$$

The dimensionless variance can be related to another dimensionless number, the Peclet number (Pe). The Peclet number is a ratio of the advective forces to dispersive forces, and is often used to characterize the hydraulic behavior of treatment wetlands. The Peclet number is inversely related to the dimensionless variance, with a high Peclet number indicating that advective forces dominate over dispersion. From the Peclet number, the previously calculated mean velocity and the reach length, it is possible to estimate the longitudinal dispersion (D_x) within the reach.

$$\sigma_\theta{}^2 = \frac{2}{Pe} - \frac{2}{Pe^2}\left(1 - e^{-Pe}\right) \tag{2-18}$$

$$Pe = \frac{uL}{D} \tag{2-19}$$

An alternative (but very similar) method for estimating the longitudinal dispersion based on the variance of the breakthrough curve is described by Murphy (et al. 2007). Rather than calculating the dimensionless variance, this method directly calculates the

longitudinal variance (σ_x^2), and then uses an approximation of equation (1-1) to directly calculate the estimated longitudinal dispersion within the reach.

$$\sigma_x^{\,2} = \sigma_t^{\,2} u^2 \tag{2-20}$$

$$D = \frac{\sigma_x^{\,2}}{2\tau} \tag{2-21}$$

This analysis was also performed, and it was found that the difference in estimated longitudinal dispersion predicted by each method differed by less than ten percent for all reaches. It is important to realize that the estimated longitudinal dispersion obtained from the moment analysis of the breakthrough curve will be higher than the dispersion coefficient obtained from the advection dispersion and storage model (described below) because the moment analysis ascribes all variation in the breakthrough curve to dispersion and neglects the dispersive effects of transient storage.

Advection, Dispersion and Storage Model

The one dimensional advection dispersion and storage equation (1-2) was discussed in the previous chapter. Because of the difficulty of solving this partial differential equation containing spatial and temporal derivatives, it is usually easiest to solve by estimating the spatial derivatives using a finite difference approach (Runkel 1998). Each reach can be broken up into a finite number of segments (n). The length of each segment (Δx) is equal to the total reach length divided by the number of segments.

$$\Delta x = \frac{L}{n} \tag{2-22}$$

The concentrations within each segment can then be solved for, and the process iterated over a finite time step (Δt). The discrete form of the ADS equations are shown below:

$$C_{t,x} = \left[C_{t-1,x} + \left(-\frac{Q}{A}\right)\left(\frac{C_{t-1,x+1}-C_{t-1,x-1}}{2\Delta x}\right) + D\left(\frac{(C_{t-1,x+1}-C_{t-1,x})-((C_{t-1,x}-C_{t-1,x-1})}{\Delta x^2}\right) + \alpha\left(C_{St-1,x-1} - C_{t-1,x}\right)\right] * \Delta t \quad (2\text{-}23)$$

$$C_{St} = \left[C_{St-1} + \alpha\left(\frac{A}{A_S}\right)(C_{t-1} - C_{St-1})\right] * \Delta t \quad (2\text{-}24)$$

The concentration at the current time and segment is therefore a function of the concentration at that segment during the previous time step, the upstream segment concentration during the previous time step, and the upstream segment concentration at the current time step. Using Microsoft Excel (2007), a spreadsheet model was created which solves for the concentration in each segment during each time from concentrations in the appropriate adjacent cells.

Plotting the concentration in a given segment with respect to time creates a modeled breakthrough curve for that location. The modeled breakthrough curves for the segment locations corresponding to the fluorometer locations for each river were plotted side by side with the actual breakthrough curves from the tracer tests. The initial boundary concentrations in the upstream-most segment, and each of the coefficients (Q, A, D, α, and A_S) are variables which determine the position and shape of the modeled breakthrough curves. The initial boundary concentrations were known based

on the mass of tracer released and the measured river discharge. While both the discharge and channel cross sectional area were measured, the channel cross sectional area was left as an unknown to see if it would converge on the measured channel area or a smaller value reflecting the displacement effects of the vegetation bed volume. This decreased the unknowns which determine the shape of the modeled breakthrough curve to four coefficients (A, D, α, and A_S). By using the solver function in Excel to minimize the sum of squared errors between the modeled breakthrough curve and the actual breakthrough curve from the tracer test, the optimal coefficients for each reach were determined.

It is possible that two or more storage zones with different spatial and temporal characteristics are acting concurrently on the solute transport. An example in the case of spring-fed karst rivers would be simultaneous vegetation bed and hyporheic storage. In this case, it might be appropriate to model the system with a modified ADS equation which contains two storage components.

$$\frac{\partial C}{\partial t} = -u\frac{\partial C}{\partial x} + D\frac{\partial^2 C}{\partial x^2} + \alpha_A(C_{SA} - C) + \alpha_B(C_{SB} - C) \tag{2-25}$$

$$\frac{\partial C_{SA}}{\partial t} = \alpha_A \frac{A}{A_{SA}}(C - C_{SA}) \tag{2-26}$$

$$\frac{\partial C_{SB}}{\partial t} = \alpha_A \frac{A}{A_{SB}}(C - C_{SB}) \tag{2-27}$$

This will increase the number of unknowns by two: a second storage zone cross sectional area (A_{SB}) and a second exchange coefficient (α_B). To determine whether adding additional variables to improve the model fit was justified, the Akaike information criterion was used. The Akaike information criterion uses the residual sum of squares

(RSS), the number of parameters (k) and the number of observations (n) to calculate the Akaike information criterion (AIC), which ranks models according to their accuracy while penalizing the number of parameters (Akaike 1974). If the single storage zone model had a lower AIC it was used over the two storage zone model.

$$\mathrm{AIC} = 2\mathrm{k} + \mathrm{n} * \ln(\mathrm{RSS}) \tag{2-28}$$

To determine which morphologic and vegetative properties control the hydraulic properties regressions were performed comparing all of the measured morphologic properties of each river reach to both the moment analysis data and the ADS model coefficients for that reach to determine if there was a significant correlation based on the R-squared values. All of the regressions performed were linear, with the exception of the DHG regressions which were exponential as discussed earlier.

To address the hypothesis that the channel geometry controls the magnitude of dispersion, the dispersion coefficient from the ADS model was regressed against the mean hydraulic radius normalized to the discharge (R/Q). The reasoning behind this is that with a smaller hydraulic radius, more of the flow will be in contact with the bed surface creating more dispersion. The dispersion coefficient was also be regressed against the mean velocity, with the reasoning being that channel cross sectional area is a major factor controlling the velocity, and a higher mean velocity will result in greater shear stress and a greater variation in the vertical velocity profile.

To address the hypothesis that vegetation controls the magnitude of dispersion, the dispersion coefficient from the ADS model was regressed against the measure vegetation in both absolute terms (vegetation cross-sectional area) and relative terms (percentage of the total channel cross-sectional area vegetated).

To address the hypothesis that transient storage was primarily due to vegetation beds and that sediment storage was negligible, the storage zone cross-sectional area from the ADS model was regressed against the measured vegetation cross-sectional area, the sediment cross-sectional area, and the sum of the vegetation and sediment cross-sectional area.

Figure 2-1. Locations of the study sites. Alexander Creek (A), Blue Spring (B), Ichetucknee River and Mill Pond Spring (C) and Juniper Creek (D), Rainbow River (E), Rock Springs Run (F), Silver River (G), and Weeki Wachee River (H).

Figure 2-2. Site maps of the study sites. Alexander Creek (A), Blue Spring (B), Ichetucknee River and Mill Pond Spring (C) and Juniper Creek (D), Rainbow River (E), Rock Springs Run (F), Silver River (G), and Weeki Wachee River (H).

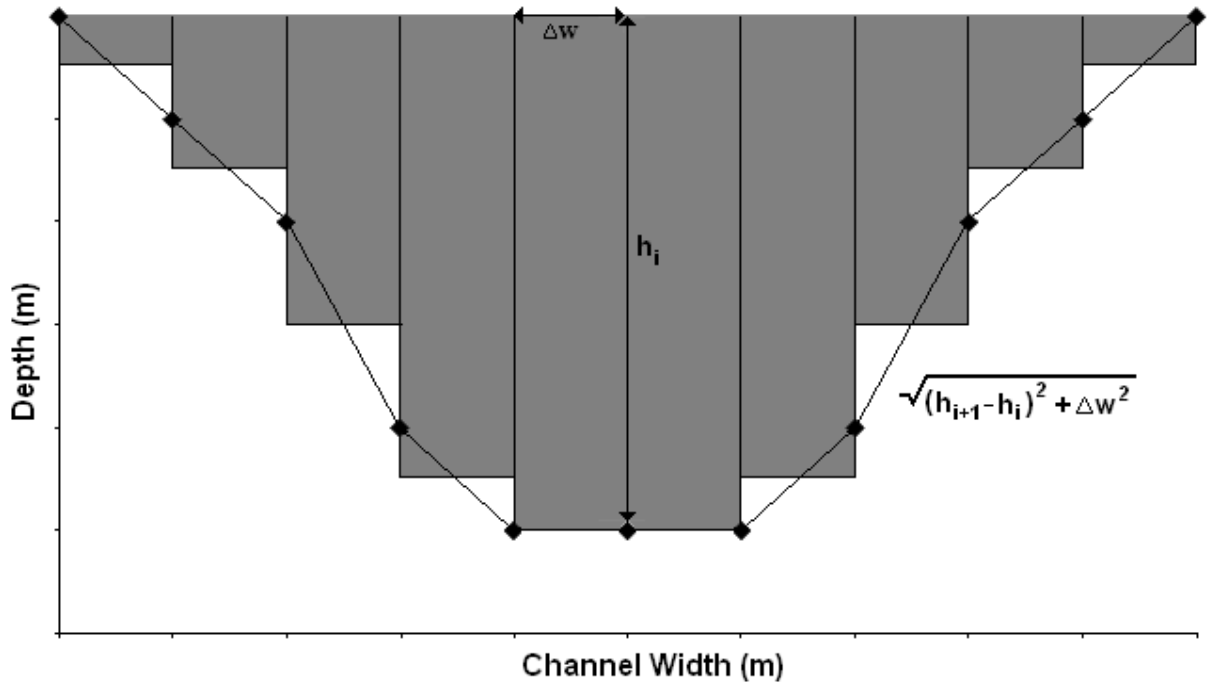

Figure 2-3. Discretized channel profile.

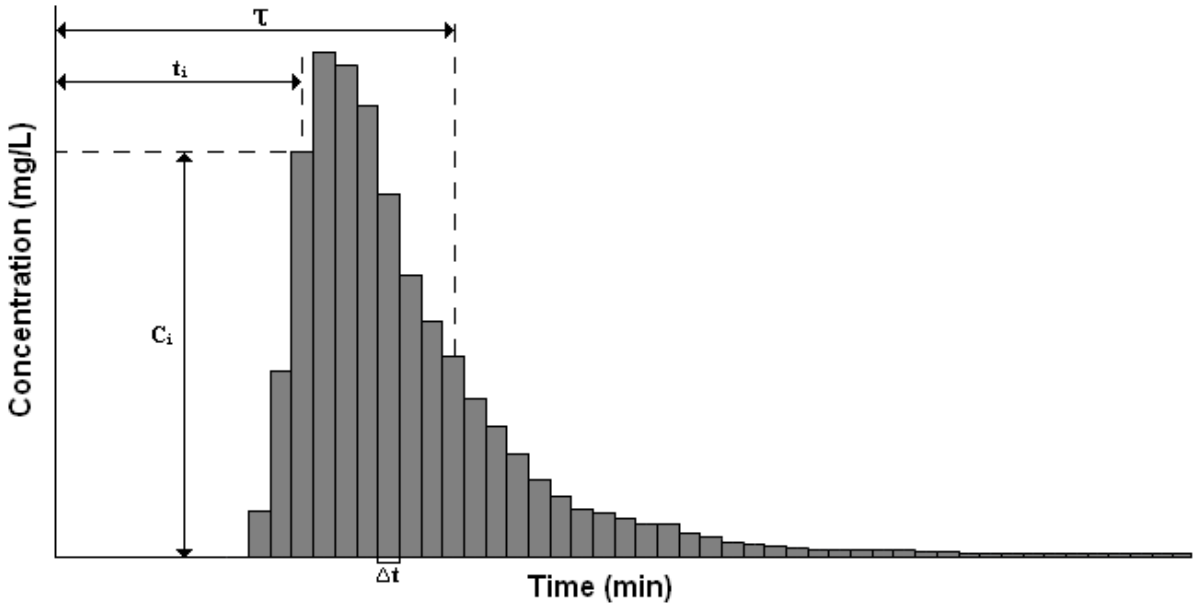

Figure 2-4. Discretized breakthrough curve.

CHAPTER 3
RESULTS

River Characteristics

There was a great deal of variability in discharge across rivers and substantial variation in morphologic and vegetative characteristics both across and within rivers (Table 3-1). The discharge across study sites ranged from 0.9 m^3/s to 16.8 m^3/s. The mean channel width ranged from 9.0 m to 65.7 m, and the hydraulic radius (effectively mean depth) ranged from 0.4 m to 2.2 m. The mean channel width correlated with the discharge (Figure 3-1), as did the mean hydraulic radius (Figure 3-2). The mean velocities will be discussed in detail in the moment analysis section however at this time it is important to note that the mean velocity also correlated with discharge (Figure 3-3), although not significantly.

A power law function was used to describe the relationship between these three parameters (width, hydraulic radius and velocity) and discharge, based on the DHG equations. The mean channel width and discharge relationship, mean hydraulic radius and discharge relationship, and the mean velocity and discharge relationship were partitioned into relationships for the upstream and downstream reaches (Figure 3-4, Figure 3-5 and Figure 3-6 respectively). The DHG coefficients and exponents for the total river relationships and the upstream and downstream reach relationships are shown in Table 3-2. The products of the coefficients and the sums of the exponents equal one as expected from the DHG equations, however note that the magnitude of the exponents are different, indicating different relationships in the upstream versus downstream reaches. The width exponent (b) is greater for the upstream reaches while the depth coefficient (f) is greater for the downstream reaches, indicating that as

discharge increases the upstream reaches get wider at a greater rate while the downstream reaches get deeper at a greater rate. This difference in channel geometry is evident in the sample channel profiles from the Ichetucknee River, where discharge remained essentially the same in both reaches (Figure 3-7). Note the distinct difference between the upstream reach (Transects nine and eight) and the downstream reach (Transects six and five); these reaches have the same channel cross-sectional area, but dramatically different widths and vegetation cross-sectional area.

The mean channel cross sectional area ranged from 4.1 m^2 to 106.2 m^2. The vegetation cross sectional area ranged from 0.0 m^2 to 34.0 m^2, and in terms of percentage of the total cross sectional area from 0% (Weeki Wachee) to 96.9% (Gilchrist Blue). The mean underlying sediment cross sectional area ranged from 8.7 m^2 to 114.3 m^2, and in relation to the channel cross-sectional area from 26.7% as large to 398.0% as large. The sediment hydraulic conductivity ranged from 2.7 m/day to 15.4 m/day, which is characterized as semi-pervious, typical of sand and silts.

Moment Analysis

The breakthrough curve moment analysis data (Table 3-3) also reflects substantial variation between rivers. Note that the moment data derived from the downstream breakthrough curve corresponds to the total of both the upstream and downstream reaches, from the tracer release point to the downstream boundary. The mean residence time can be calculated for the downstream reach however, by subtracting the mean residence time of the upstream reach from the mean residence of the combined reaches.

The mean residence time ranged from 19.2 minutes to 685.0 minutes. The mean residence time alone is somewhat meaningless however, because each reach is a

different length. Dividing the reach length by the mean residence time gives the mean velocity which ranged from 0.03 m/s to 0.28 m/s. The mean velocity correlated strongly with the expected mean velocity calculated by dividing the discharge by the channel area (Figure 3-8). There was also a correlation between the mean velocity and the fraction of the channel cross sectional area vegetated (A_V/A), with the mean velocity decreasing as the percentage of the channel vegetated increased (Figure 3-9). The correlation between the moment derived dispersion and the mean velocity (Figure 3-10) was also positive indicating that a higher velocity creates more shear stress dispersion.

Advection Dispersion and Storage Model Analysis

The breakthrough curves and the fitted ADS model curves for the upstream and downstream reaches of each river are shown in Figure 3-11. These same curves are shown vs. log-concentration in Figure 3-12 to accentuate the long-residence time flowpaths. The breakthrough curve and fitted model curve for the continuous tracer test for Mill Pond Spring are shown in Log-space in Figure 3-13. Many of the breakthrough curves have pronounced long tails which become apparent in Log-space (e.g., Ichetucknee upper). Notice how the ADS model, even when two storage zones are used, many times fails to adequately fit the tail (e.g., Blue upper, Juniper upper and lower, Rock upper). The possible causes of this will be discussed in detail in the Discussion chapter.

The optimal coefficients for the ADS model are shown in Table 3-4. In cases where a two storage zone model did not significantly improve the fit of the breakthrough curve, the second storage zone cross sectional area and exchange coefficient are listed as Not Applicable (NA).

The ADS model was also run for the entire river as a single reach. These values were only used for comparison with moment derived values for the entire river. Because the morphology of the entire river is a composite of the upstream and downstream reaches, the coefficients from the model of the entire river as a single reach were not used in the regression, so as not to be redundant. The ADS model dispersion coefficients for the upstream reach and the entire river correlated very strongly with their corresponding moment dispersion estimations (Figure 3-14), despite the fact that the magnitudes were different because the moment based calculation attributed all variance to dispersion.

The ADS model channel cross sectional area correlated very strongly with the measured channel cross sectional area (Figure 3-15) however the ADS model channel cross-sectional area was approximately 15% smaller than the measured channel cross-sectional area.

The ADS model dispersion coefficient was weakly negatively correlated with the hydraulic radius normalized for discharge (R/Q) (Figure 3-16). The ADS model dispersion coefficient was also weakly negatively correlated with the channel cross-sectional area normalized for discharge (A/Q) (Figure 3-17). The ADS model dispersion coefficient was strongly correlated with the measured mean velocity (Figure 3-18). The ADS model dispersion coefficient did not however correlate with the vegetation cross sectional area as expected (Figure 3-19) and was even weakly negatively correlated with the fraction of the channel vegetated (Figure 3-20).

The total model storage zone cross sectional area ($A_{SA} + A_{SB}$) correlated strongly with the vegetation cross sectional area (Figure 3-21), however the sediment cross

sectional area correlated even stronger (Figure 3-22). The cross-sectional area of each individual storage zone (A_{SA} or A_{SB}) also correlated with both vegetation cross-sectional area and sediment cross-sectional area; however these are not shown as the total storage area (A_{SA} or A_{SB}) correlated just as well, only the slope was different. The strongest correlation was between the total model storage cross sectional area (A_{SA} + A_{SB}) and the sum of vegetation cross-sectional area and sediment cross-sectional area (A_V + A_H) (Figure 3-23).

For the breakthrough curves and fitted ADS model curves for the Blue Spring under varying vegetation conditions (Figure 3-24) notice that the breakthrough curve for the tracer test during high vegetation has a longer residence time and a much more pronounced tail. The optimal coefficients for the one dimensional advection dispersion and storage model under both vegetative conditions are shown in Table 3-5. Note that the dispersion coefficient was nearly identical under both vegetative conditions. The storage zone cross-sectional area is actually larger in the case of lower vegetation, however the exchange coefficient is also greater meaning the storage zone empties rather quickly and does not produce the long tail observed in the case of higher vegetation.

Table 3-1. Summary of morphologic and vegetative characteristics.

River Reach	Q (m^3/s)	L (m)	W (m)	R (m)	A (m^2)	A_V (m^2)	A_H (m^2)	K (m/d)
Alexander Creek US	3.8	1300	34.6	1.0	33.7	4.1	55.4	4.4
Alexander Creek DS	4.5	1800	62.8	0.8	46.4	22.7	82.8	4.0
Alexander Creek Total	-	3100	48.7	0.9	40.1	13.4	69.1	4.2
Blue Spring US	0.9	140	28.0	1.0	26.7	25.9	27.1	2.7
Blue Spring DS	1.1	210	18.8	0.6	10.8	7.4	27.1	2.7
Blue Spring Total	-	350	22.3	0.7	16.3	13.6	27.1	2.7
Ichetucknee River US	6.5	1800	62.6	0.7	33.2	17.3	86.4	4.6
Ichetucknee River DS	6.5	2500	24.0	1.2	31.3	10.7	19.4	5.4
Ichetucknee Total	-	4300	43.3	1.0	32.3	14.4	52.9	5.0
Juniper Creek US	1.3	1700	9.0	0.5	4.1	0.2	16.3	4.2
Juniper Creek DS	1.7	1000	9.8	1.0	10.2	0.0	19.9	8.1
Juniper Creek Total	-	2700	9.4	0.7	7.2	0.1	18.1	5.9
Mill Pond Spring	0.9	160	10.8	0.4	4.8	3.2	8.7	-
Rainbow River US	14.7	1500	65.7	1.5	106.2	32.6	28.4	6.1
Rainbow River DS	16.8	4250	47.8	1.4	65.9	12.4	20.7	4.6
Rainbow River Total	-	5750	56.7	1.4	86.1	22.5	24.5	4.3
Rock Springs Run US	1.3	700	8.0	0.6	5.2	0.0	11.8	15.4
Rock Springs Run DS	1.3	2300	35.3	0.6	23.6	13.2	47.4	4.0
Rock Springs Total	-	3000	23.6	0.6	15.7	7.5	32.1	8.9
Silver River US	14.5	1550	47.1	2.2	101.9	34.0	114.3	4.2
Silver River DS	15.5	5300	30.9	2.2	71.3	20.7	63.2	3.5
Silver River Total	-	6850	36.3	2.2	81.5	25.1	80.3	3.7
Weeki Wachee US	3.1	1300	21.5	0.6	15.0	1.5	48.1	5.6
Weeki Wachee DS	3.1	2000	12.0	0.8	8.8	0.0	26.6	9.6
Weeki Wachee Total	-	3300	17.2	0.7	12.2	0.8	37.3	7.6

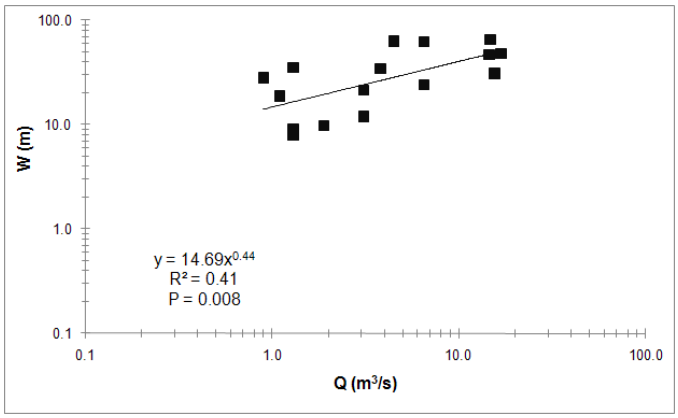

Figure 3-1. Correlation between mean channel width (W) and discharge (Q).

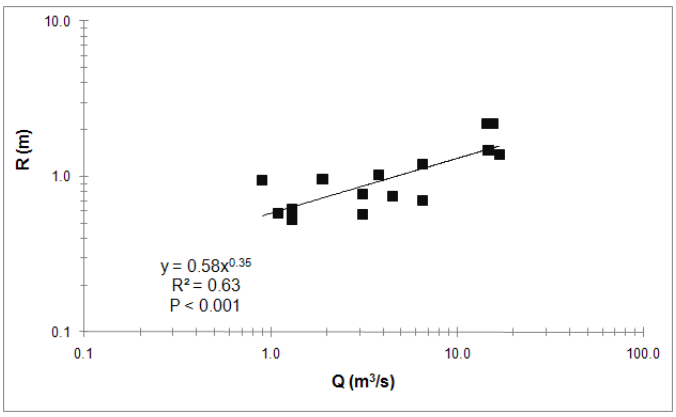

Figure 3-2. Correlation between mean hydraulic radius (R) and discharge (Q).

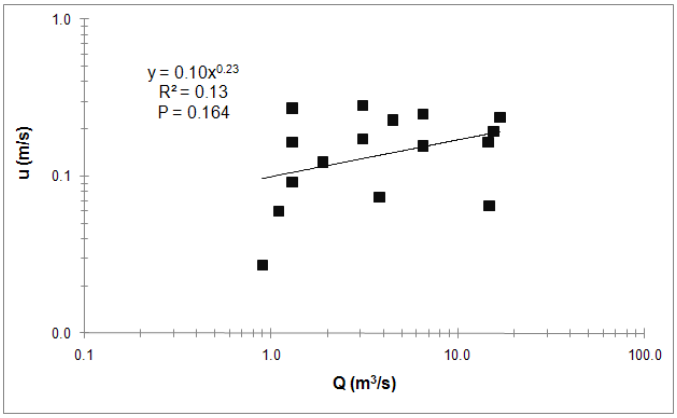

Figure 3-3. Correlation between mean velocity (u) and discharge (Q).

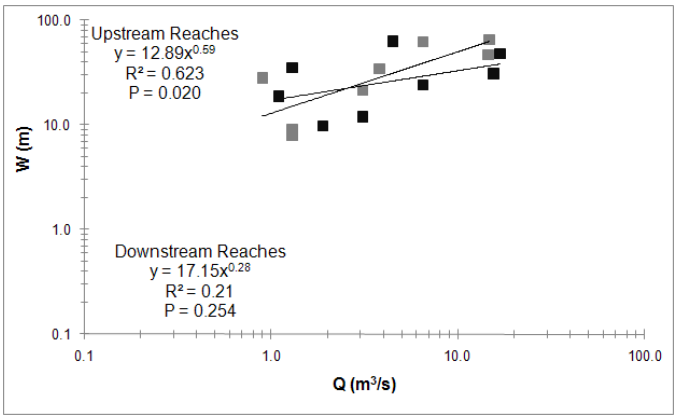

Figure 3-4. Correlations between mean channel width (W) and discharge (Q), separated into upstream and downstream reaches.

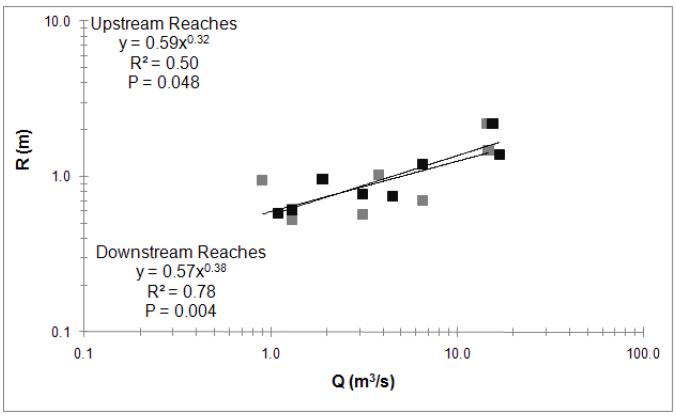

Figure 3-5. Correlations between mean hydraulic radius (R) and discharge (Q), separated into upstream and downstream reaches.

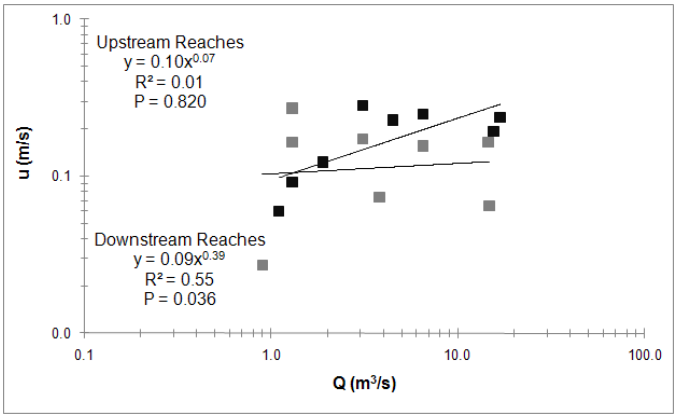

Figure 3-6. Correlations between mean velocity (u) and discharge (Q), separated into upstream and downstream reaches.

Table 3-2. Summary of DHG coefficients and exponents

River Reach	c1	c2	c3	b	f	m
Total Rivers	14.15	0.56	0.10	0.46	0.37	0.21
Upstream Reaches	12.89	0.59	0.10	0.59	0.32	0.07
Downstream Reaches	17.15	0.57	0.09	0.28	0.38	0.39

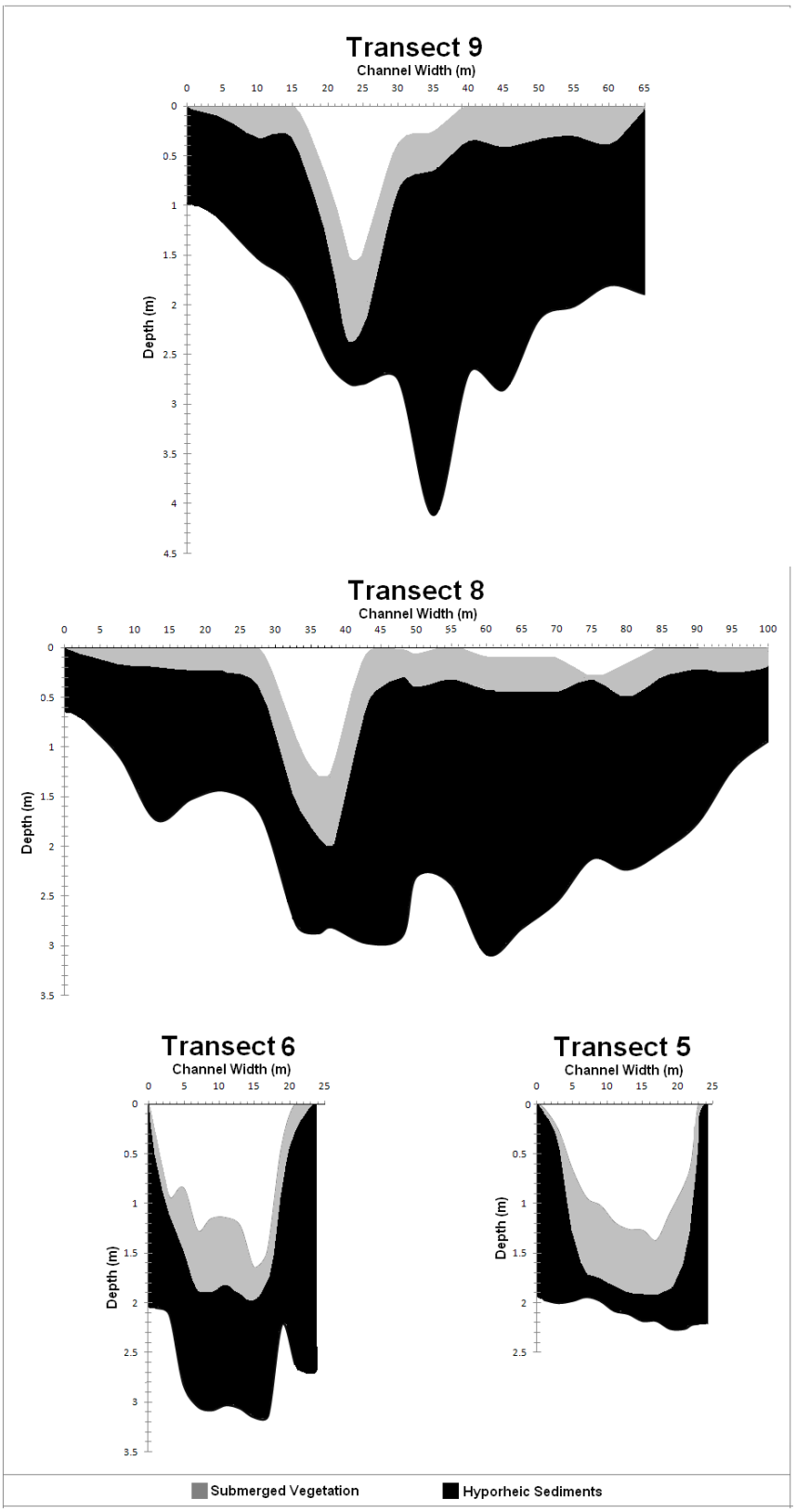

Figure 3-7. Sample channel profiles for Ichetucknee River.

Table 3-3. Summary of breakthrough curve moment analysis.

River Reach	Mass Recovery	Residence Time (min)	Velocity (m/s)	D (m^2/s) (Kadlec)	D (m^2/s) (Murphy)
Alexander Creek US	99.9%	293.7	0.07	7.9	7.2
Alexander Creek DS	-	131.6	0.23	-	-
Alexander Creek Total	100.2%	607.3	0.09	5.4	5.6
Blue Spring US	104.5%	86.0	0.03	0.3	0.3
Blue Spring DS	-	58.8	0.06	-	-
Blue Spring Total	99.1%	144.7	0.04	1.5	1.3
Ichetucknee River US	100.2%	192.5	0.16	30.2	27.3
Ichetucknee River DS	-	168.2	0.25	-	-
Ichetucknee River Total	99.7%	360.7	0.20	36.8	35.4
Juniper Creek US	99.6%	172.4	0.16	26.1	23.7
Juniper Creek DS	-	135.4	0.12	-	-
Juniper Creek Total	99.5%	307.8	0.15	14.8	14.2
Mill Pond Spring	99.2%	19.2	0.14	-	-
Rainbow River US	98.9%	386.8	0.06	5.5	5.4
Rainbow River DS	-	293.3	0.24	-	-
Rainbow River Total	97.5%	685.0	0.14	15.6	15.4
Rock Springs Run US	100.5%	43.0	0.27	15.9	14.6
Rock Springs Run DS	-	418.4	0.09	-	-
Rock Springs Total	79.5%	461.4	0.11	9.0	8.7
Silver River US	99.7%	156.6	0.16	14.5	13.7
Silver River DS	-	456.2	0.19	-	-
Silver River Total	96.1%	612.8	0.19	28.6	28.0
Weeki Wachee River US	99.3%	125.5	0.17	17.8	16.4
Weeki Wachee River DS	-	118.1	0.28	-	-
Weeki Wachee Total	101.3%	243.6	0.23	9.4	9.2

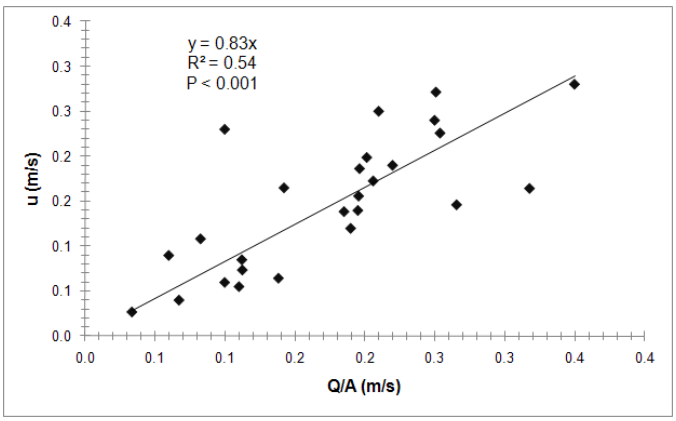

Figure 3-8. Correlation between mean velocity (u) and expected velocity (Q/A).

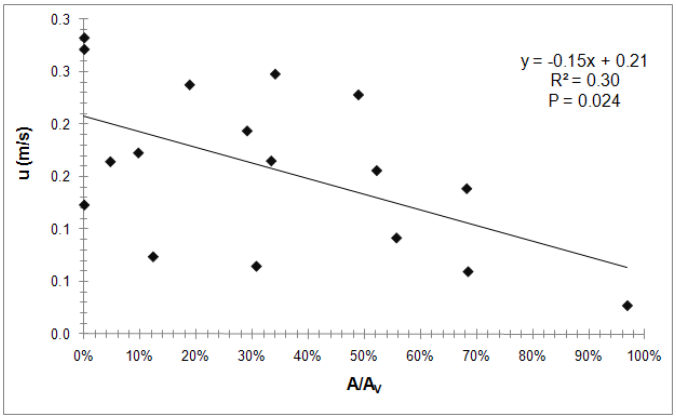

Figure 3-9. Correlation between mean velocity (u) and percentage of the channel cross sectional area vegetated (A_V/A).

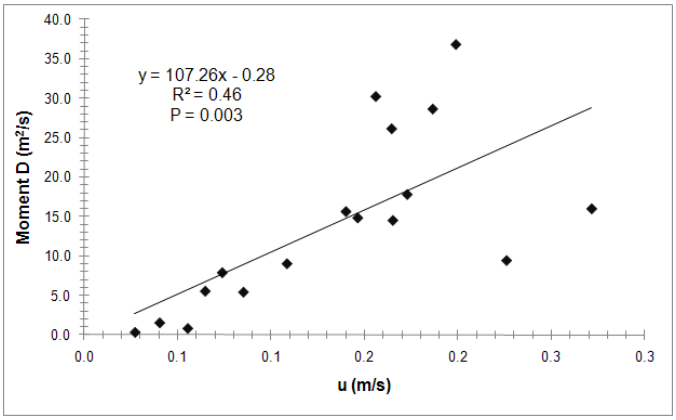

Figure 3-10. Correlation between moment based dispersion (D) and mean velocity (u).

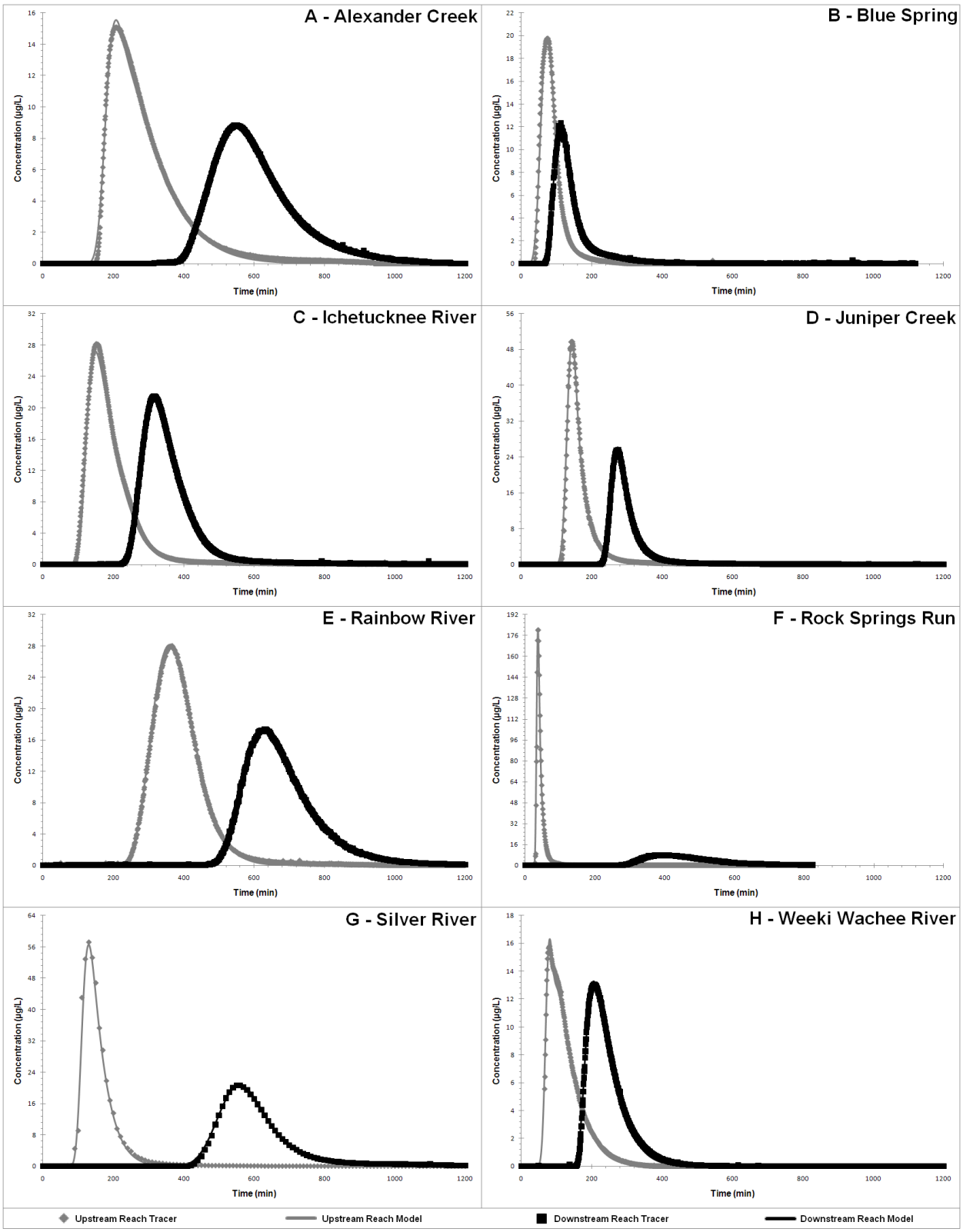

Figure 3-11. Tracer breakthrough curves and fitted model curves.

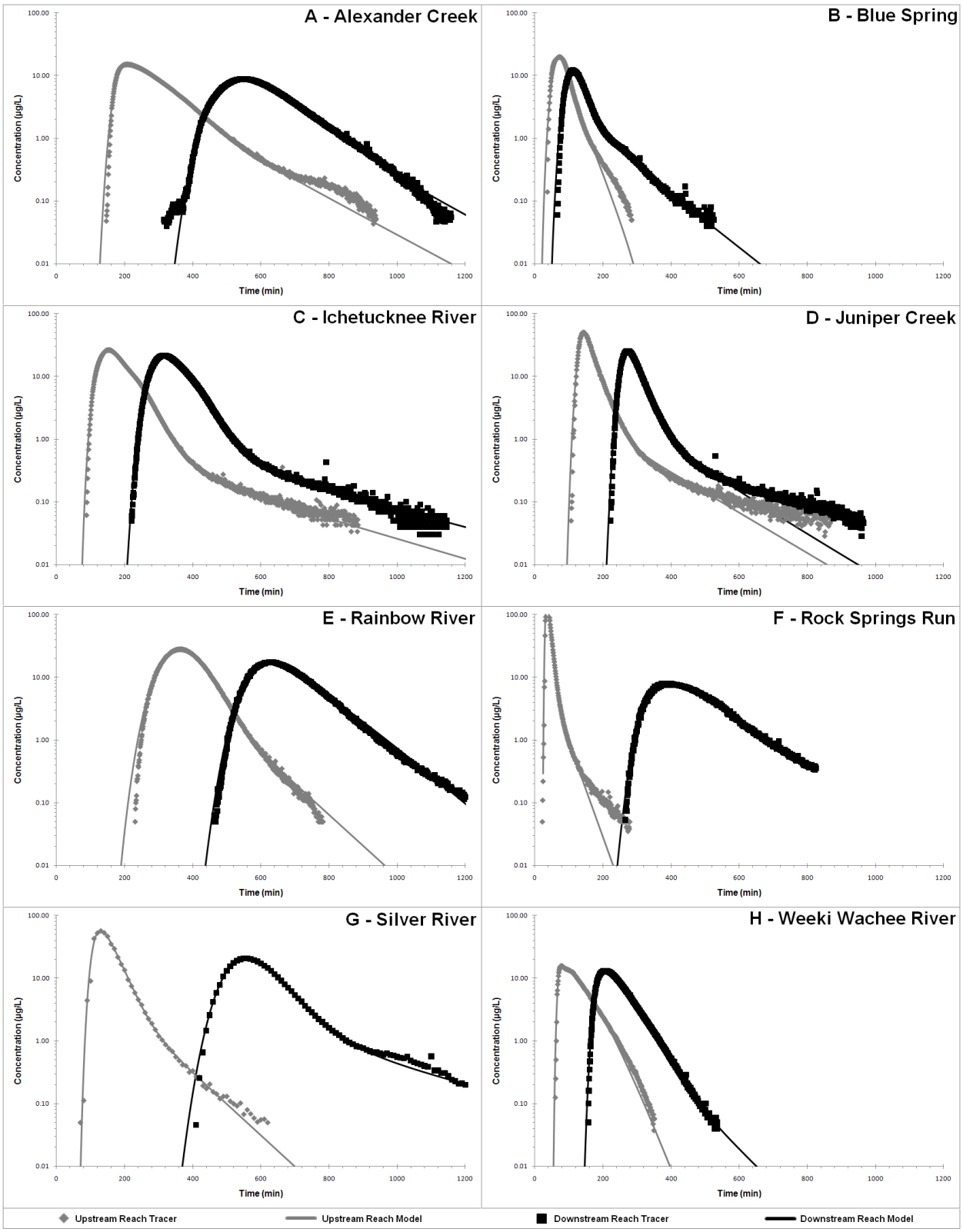

Figure 3-12. Tracer breakthrough curves and fitted model curves in Log-space.

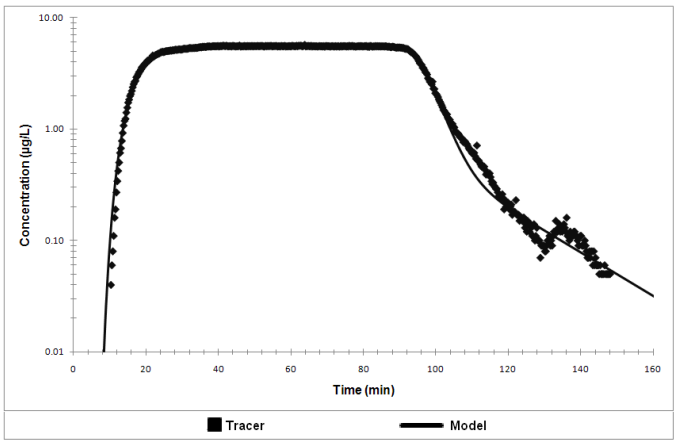

Figure 3-13. Mill Pond Spring continuous injection tracer breakthrough curve and fitted model curve in Log-space.

Table 3-4. Summary of advection dispersion and storage model coefficients.

River Reach	A (m^2)	A_{SA} (m^2)	A_{SB} (m^2)	D (m^2/s)	α_A (1/s)	α_B (1/s)	RSS
Alexander Creek US	31.9	11.2	7.6	0.7	0.00022	0.00004	16.5
Alexander Creek DS	41.6	2.5	NA	2.4	0.00002	NA	4.3
Alexander Creek Total	36.4	7.6	4.7	1.7	0.00021	0.00003	2.5
Blue Spring US	25.2	5.1	NA	0.1	0.00024	NA	78.7
Blue Spring DS	12.3	7.5	NA	0.6	0.00012	NA	7.8
Blue Spring Total	20.1	4.2	NA	0.4	0.00005	NA	7.7
Ichetucknee River US	25.44	5.1	2.5	7.8	0.00011	$3.4x10^{-6}$	21.1
Ichetucknee River DS	21.8	1.7	1.8	5.6	0.00008	$3.0x10^{-6}$	6.1
Ichetucknee Total	24.4	5.5	1.7	5.8	0.00010	$4.1x10^{-6}$	5.4
Juniper Creek US	6.4	0.8	0.5	2.4	0.00012	0.00001	150.87
Juniper Creek DS	10.9	1.4	0.9	0.4	0.00028	0.00001	7.8
Juniper Creek Total	7.9	0.8	0.6	1.3	0.00015	0.00001	11.7
Mill Pond Spring	5.8	0.8	NA	1.0	0.00015	NA	5.4
Rainbow River US	122.2	10.1	4.8	3.3	0.00008	$3.5x10^{-6}$	18.2
Rainbow River DS	53.5	12.7	NA	1.2	0.00007	NA	20.8
Rainbow River Total	74.0	15.2	5.1	2.6	0.00014	0.00001	19.3
Rock Springs Run US	3.9	0.6	0.1	4.0	0.00044	0.00002	1005.0
Rock Springs Run DS	10.7	15.6	4.3	1.3	0.00002	0.00018	8.2
Rock Springs Total	9.3	10.9	3.2	2.1	0.00001	0.00015	7.9
Silver River US	57.8	12.0	8.3	1.8	0.00061	0.00004	200.9
Silver River DS	62.3	11.2	6.2	4.5	0.00014	0.00001	6.6
Silver River Total	64.4	11.8	5.3	4.7	0.00015	0.00001	4.2
Weeki Wachee US	9.1	5.6	NA	3.8	0.00049	NA	20.5
Weeki Wachee DS	8.8	0.4	NA	5.7	0.00001	NA	6.6
Weeki Wachee Total	9.1	2.2	NA	5.2	0.00018	NA	8.8

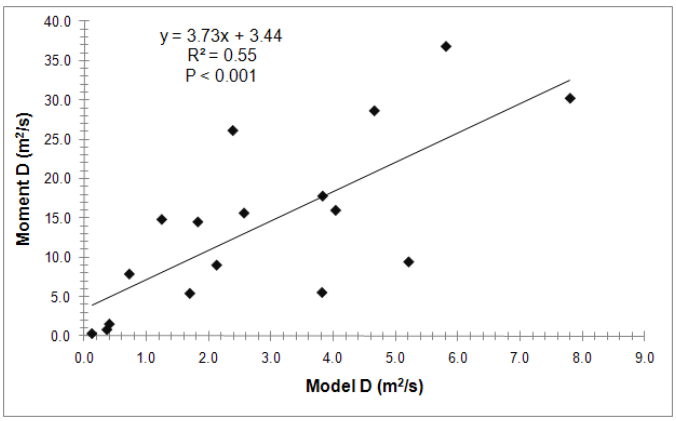

Figure 3-14. Correlation between moment derived dispersion estimation and ADS model dispersion coefficient.

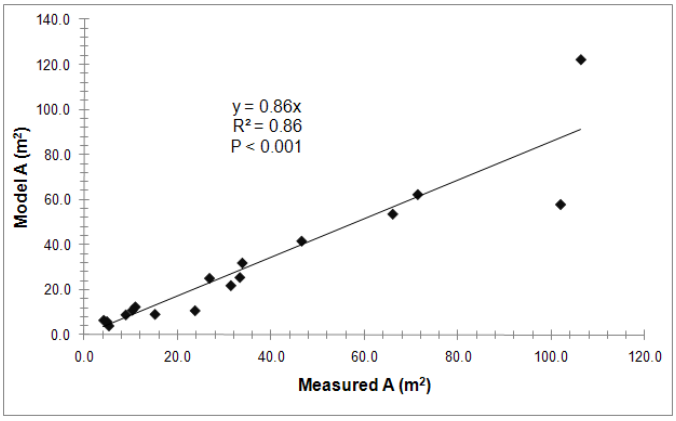

Figure 3-15. Correlation between ADS model channel cross sectional area and measured channel cross sectional.

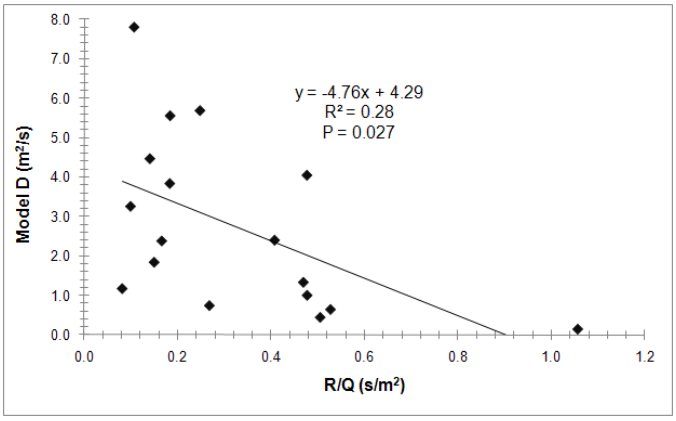

Figure 3-16. Correlation between ADS model dispersion coefficient and the hydraulic radius normalized for discharge (R/Q).

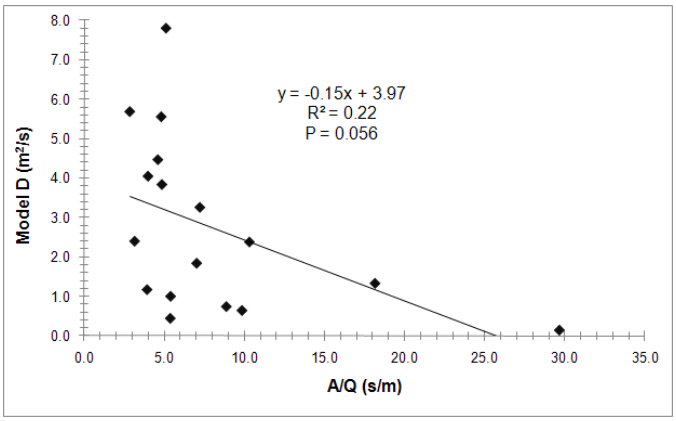

Figure 3-17. Correlation between ADS model dispersion (D) and the channel area normalized for discharge (A/Q).

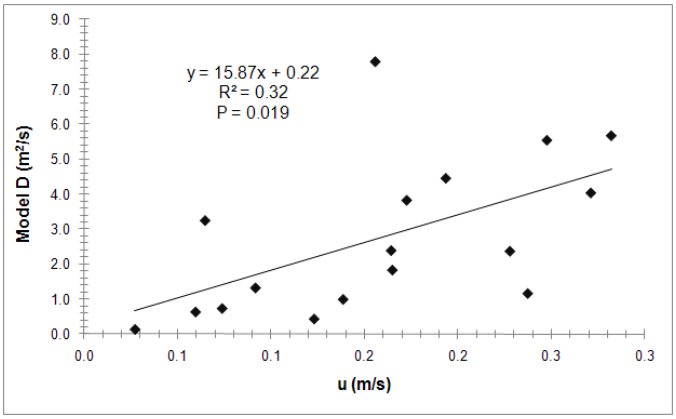

Figure 3-18. Correlation between ADS model dispersion (D) and measured velocity (u).

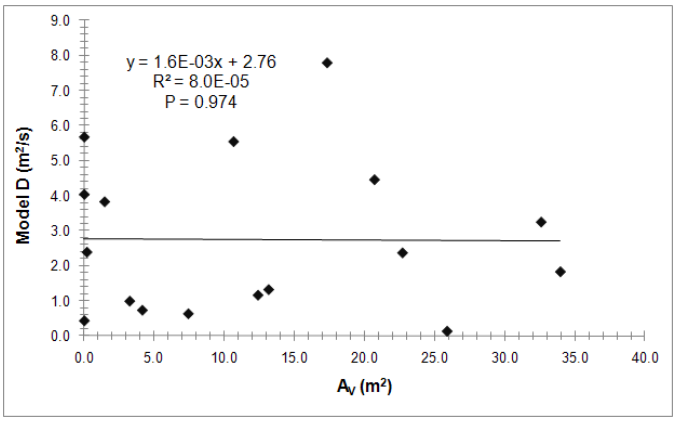

Figure 3-19. Correlation between ADS model dispersion (D) and vegetation cross sectional area (A_V).

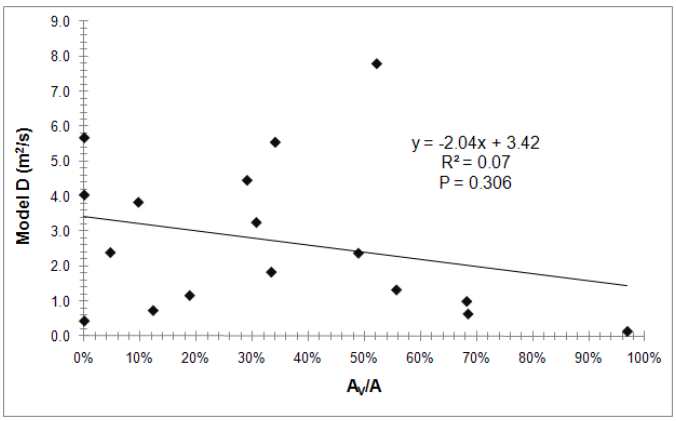

Figure 3-20. Correlation between ADS model dispersion (D) and percent vegetation cross sectional area (A_V/A).

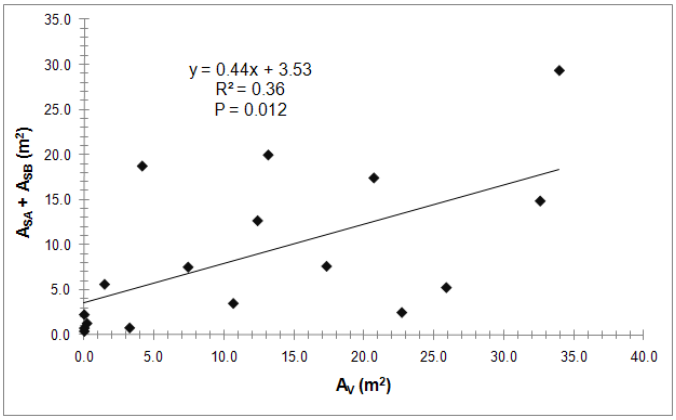

Figure 3-21. Correlation between ADS model total storage zone cross sectional area (A_{SA}) and vegetation cross sectional area (A_V).

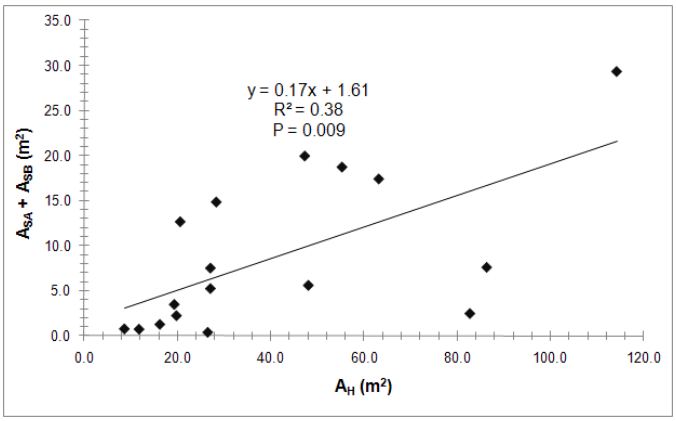

Figure 3-22. Correlation between ADS model total storage zone cross sectional area (A_{SA}) and sediment cross sectional area (A_H).

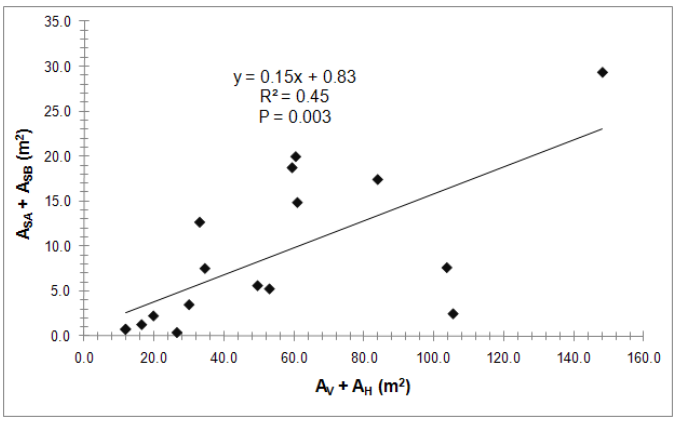

Figure 3-23. Correlation between ADS model total storage zone cross sectional area ($A_{SA} + A_{SB}$) and the sum of vegetation and sediment cross sectional areas ($A_V + A_H$).

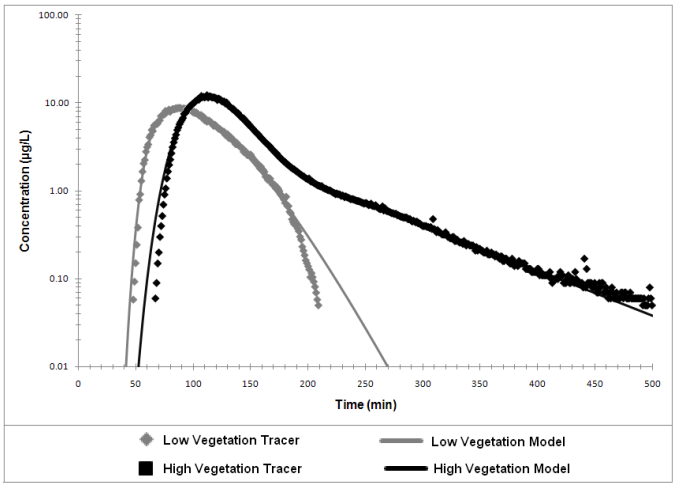

Figure 3-24. Blue Spring tracer breakthrough curves and fitted model curves under varying vegetative conditions in Log-space.

Table 3-5. Summary of ADS model coefficients for Blue Spring under varying vegetative conditions.

River Reach	A (m^2)	A_{SA} (m^2)	A_{SB} (m^2)	D (m^2/s)	α_A (1/s)	α_B (1/s)	RSS
Blue Spring High Veg.	20.1	4.2	NA	0.4	0.00005	NA	7.7
Blue Spring Low veg.	15.7	9.0	NA	0.4	0.00085	NA	5.1

CHAPTER 4
DISCUSSION

Morphologic and Vegetative Characteristics

This study is the first to characterize the hydraulic properties of Florida's spring-fed rivers, a knowledge gap made notable in light of their broad utility as riverine model systems. Among the sentinel advancements in lotic ecosystem ecology in the last 20 years is the recognition of the important control that channel hydraulics exerts on the flora and fauna that can persist in a river, on ecosystem production and respiration, and on the processing of nutrients. Because understanding these ecological elements of spring-fed rivers is a pressing priority, providing baseline hydraulic information fills a critical knowledge gap.

Across rivers, the mean channel width, the hydraulic radius and the mean velocity correlated with discharge through a power law relationship, consistent with previous studies (Leopold et al. 1953, Leopold et al. 1964, Park 1977). The product of the coefficients and the sum of the exponents were also approximately equal to one. However, while the observations on channel geometry across the study sites conform well to previous observations from other river systems, there are unique differences when making observations within study sites.

In general, as discharge (and the distance downstream) increases, the channel width increases at a greater rate than depth (Leopold et al. 1953). This was not the case in the studied rivers. Of the eight study sites with upstream and downstream reaches, only two (Alexander Creek and Rock Springs Run) displayed any increase in channel width. The width of Juniper Creek increased slightly, but was accompanied by a much larger increase in depth. The other five sites actually showed a decrease in

channel width. Mill Pond was not divided into upstream and downstream reaches, however the individual transects show a decrease in channel width with downstream distance. Additionally, the spring pools, and often the upstream most portions of many of these rivers were not included in the study. Visual observations indicate that including these areas would amplify this deviation from expected behavior, even in the cases of Alexander Creek and Rock Springs Run.

The product of the DHG coefficients and the sum of the DHG exponents for both the upstream and downstream data sets still approximately equal one, however the relationships between these geometric properties are quite different. For the upstream data set, the width coefficient b (0.59) is greater than the depth coefficient f (0.32) indicating that as discharge increases the width increases at a greater rate than the depth, typical of the behavior observed in other river systems as discussed above. For the downstream data set however, the width coefficient b (0.28) is less than the depth coefficient f (0.38) indicating that the depth increases at a greater rate than the width, consistent with the observations. The velocity coefficient is also much greater for the downstream data set indicating that the velocity increases with discharge at a much greater rate than in the upper reaches. Looking at the P-values, the channel width is more significantly correlated with discharge in the upstream reach, while depth and velocity are more significantly correlated with discharge in the downstream reach.

These differences may say something about the different forces driving channel formation in the upstream versus the downstream reach. Channel evolution in most river systems is typically controlled by scouring forces, and the channel geometry is driven by optimal energy expenditure (Leopold et al. 1953). Spring-fed rivers have a

relatively constant discharge without the high discharge pulse events observed in other river systems, so some other mechanism is probably driving channel evolution.

A possible explanation is that the channel bed slope may be different between the upstream and downstream reaches. A steeper bed slope in the downstream reaches would cause an increase in velocity as observed in the m coefficients (0.07 upstream and 0.39 downstream). Because the velocity is greater in the downstream reaches, the channel area required to convey the same discharge would be smaller, explaining why the b coefficient is smaller than in the upstream reaches.

The water emanating from a spring vent is saturated with respect to calcium carbonate, having spent many years in the aquifer equilibrating with the karst matrix. However, biological activity, specifically the processes which would be expected in the anaerobic hyporheic zone, often reduces the pH to a level where further dissolution is possible. In the upstream reaches of spring-fed rivers, the hydraulic flux may be out of the sediments (as evident by the presence of artesian springs), preventing any under-saturated water within the sediments from spending much time reacting with the bedrock. In the downstream reach this hydraulic gradient may not exist, or in the case of losing rivers such as the Ichetucknee River may be into the hyporheic sediments. Under-saturated water is able to remain in the hyporheic zone and dissolve limestone at the hyporheic-bedrock interface, causing the channel slope to increase. Additionally, many of these rivers also flow into “dark-water” rivers which unlike spring-rivers have highly variable discharge. Under peak flow conditions the pH of these dark-water rivers decreases and backwater effects can result in under-saturated water flowing up the

tributary spring-rivers (J.B. Martin, Unpublished data). This mechanism may also result in potential channel dissolution.

Limitations of the Advection, Dispersion and Storage Model

In fitting the breakthrough curves, it became apparent that particulars of model structure and fitting criteria were critical in determining the coefficients which describe the hydraulic behavior. When viewing the breakthrough curves in Log-space it became apparent that it was necessary to consider not just the properties which control the bulk of the breakthrough curve but also the tails. The tails represent the “long-time” flowpaths which are crucially import important in regard to understanding nutrient processing not just because of their residence times but because they may represent transport through physical locations (such as hyporheic zones) within the river system where specific metabolic processes (such as denitrification) may take place.

In most cases the ADS model with a single storage zone failed to fit the long tails of the breakthrough curve. Adding of a second storage zone with a smaller exchange coefficient (indicating a longer storage zone turnover time) often improved the fit. This second storage zone always had an exchange coefficient smaller than the exchange coefficient of the primary storage zone, indicating a longer storage zone turnover time, resulting in an extended tail (and often a notable break in slope) on the modeled breakthrough curve. The cross-sectional area of the second storage zone was also generally smaller than the cross-sectional area of the primary storage zone. Physically, these two storage zones may be vegetation beds (larger cross-sectional area and more rapid exchange), and the hyporheic zone (smaller cross-sectional area and slower exchange). In this study and to my knowledge all other studies which have implemented a second storage zone, exchange has been between the advective

channel and the individual storage zones. A more realistic approach may be a primary storage zone exchanging with the channel, and a secondary storage zone exchanging with the primary storage zone. This type of model would physically make more sense for a system where solutes exchange from the channel into and out of the vegetation beds, and then subsequently from the vegetation beds into and out of the underlying hyporheic sediments.

However, in some cases even the addition of a second storage zone still did not result in complete fitting of the tail of the breakthrough curve. This may arise from minimizing the squared error as the model fitting criteria rather than minimizing the absolute error. Because the concentrations in the tail are far lower than in the peak, any potential error between the tracer curve and the model curve will be minor in the tail relative to the peak. Squaring these errors will amplify the relative magnitudes (particularly when the error in the tail is less than one). Using the squared error as the model fitting criterion may thus lead to preferential fitting of the peak over the tail. While fitting the peak portion of the curve which represents the majority of the solute transport may not seem so bad, the tails may actually be of more importance. The particular flowpaths represented by the tails probably play a more direct role in nutrient cycling.

Previous studies (Choi et al. 2000) have indicated that in the majority of simulated cases, storage could be represented by a single storage zone which averaged the properties of multiple storage zones. The problem with this study and hence its conclusions is that the curves used were not real data, but were generated by the advection, dispersion and storage equation, creating a circular inference. The nature of the ADS equation results in any curve having an exponential distribution of residence

times, where a non-exponentially distributed model, such as a power-law may be more realistic for fitting actual breakthrough curves (Gooseff et al. 2003). A power-law distribution of residence times, which could physically arise from multiple storage zones, or from storage zones with variable temporal or spatial properties, provides for the possibility that some water spends far longer in the system than the mean. This yields skewed distributions with longer tails, similar to those observed in this study, suggesting that a non-exponentially distributed model may be required to adequately describe the hydraulics of these rivers.

Morphology and Vegetation as a Control on Dispersion

In addition to providing the first systematic survey of hydraulic and geometric properties of spring fed rivers, this study also tested hypotheses about the role of channel form and submerged aquatic vegetation in regulating riverine hydraulics.

It was hypothesized that the channel geometry acted as a control on the magnitude of dispersion. This study determined that the magnitude of dispersion is weakly inversely correlated with the hydraulic radius normalized for discharge and the mean channel cross-sectional area normalized for discharge. As these values decrease, a greater portion of the flow experiences boundary layer effects. This increase in shear stress due to friction causes an increase in the magnitude of dispersion. The magnitude of dispersion was also strongly positively correlated with the measured mean velocity. This is likely a result of higher velocities resulting in greater shear stress and a less uniform vertical velocity profile. It has already been well documented that channel geometry is one of the primary mechanisms controlling mean velocity in open channels (Manning 1890, Manning 1895, Chow 1959), and this study found that the observed mean velocity was highly correlated with the discharge divided

by the channel area as predicted by the continuity equation. These observations appear to support the hypothesis that channel geometry is acting as a control on the magnitude of dispersion.

In addition to channel geometry, the other main driver of open channel velocity is the amount of benthic friction (Manning 1890, Manning 1895, Chow 1959), and numerous studies have found that vegetation increases friction and is negatively correlated with velocity (Palmer 1945, Ree 1949, Kouwen et al. 1969). This was observed in this study, both as a negative correlation between vegetation and mean velocity across the study springs, and also more directly in the effect of changing vegetation on residence time (and hence mean velocity) in Blue Spring.

It was hypothesized that benthic submerged vegetation density was another mechanism controlling the magnitude of dispersion. While the presence of vegetation has been shown to induce dispersion through turbulence and non-uniform lateral velocity profiles (Nepf et al. 1997, Nepf et al. 1999, Lightbody 2006), the opposite effect was observed in this study, with vegetation being weakly inversely correlated with dispersion. An explanation of this is that the vegetation was found to be negatively correlated with velocity, and velocity was found to be positively correlated with the magnitude of dispersion as discussed above. The decrease in mean velocity due to vegetation results in decreased vertical shear stress dispersion. Additionally, the decrease in mean velocity results in decreased Reynolds number meaning the vegetation is creating less turbulence and a more uniform lateral velocity profile. So the observations do support the hypothesis that vegetation is a mechanism controlling the

magnitude of dispersion; however the correlation was negative, rather than positive as expected.

Mechanisms Controlling Transient Storage

It was hypothesized that vegetation beds acted as transient storage zones, while sediment storage was negligible, principally because of low sediment hydraulic conductivities. While the assumption that hydraulic conductivities of the sediments are uniformly low was supported by direct measurements, with values typically less than 10 m/day, inference about the relative importance of these sediments as transient storage is more complex than expected. In particular, the observation that the total model cross-sectional area correlated most strongly with the sum of vegetation and sediment cross-sectional area indicates that both storage zones are probably important. This was supported by the observation that a two storage zone model usually fit the breakthrough curve better, and the exchange coefficients for these two storage zones were significantly different. The size of the model storage zones were much smaller than the measured vegetation and sediment cross-sectional area, which indicates that any transient storage that is occurring is doing so only in a fraction of these volumes.

In the case of Blue Spring under varying vegetative conditions, the model storage cross-sectional area was actually greater for the low vegetation conditions. However, while the total storage zone cross-sectional area for the low vegetation conditions was larger, the exchange coefficient was also very large meaning the overall effect on residence time distribution was smaller than in the high vegetation case. This is evident in the comparison of the breakthrough curves, which have the same dispersion coefficient, but a greater mean residence time for the high vegetation conditions. This indicates that even though the ADS model storage zone cross-sectional area was

smaller, the effect of transient storage on the residence time distribution was greater in the high vegetation case. A very likely explanation for this is that the tracer was released directly over the spring vent which is in the center of a large pool enlarged for recreational purposes. In the low vegetation tracer test the tracer was observed to disperse out and occupy this entire pool before subsequently being advected downstream within a short amount of time. However in the case of high vegetation, the tracer was observed to be contained directly around the release point by the dense vegetation. The tracer was advected downstream very slowly through the vegetation and a small preferential flowpath. The ADS model results are consistent with these observations.

The mass recovery alone also has implications for the type of storage which is occurring. Near total mass recovery occurred in every tracer test (range was from 95 – 105%). Many previous studies using Rhodamine WT have failed to get complete mass recovery, and this is partially due to the fact that Rhodamine WT is not perfectly conservative, having a tendency to sorb to sediments (Smart et al. 1977, Bencala el al. 1983b, Sabatini et al. 1991). The accuracy of the discharge measurement used can have a significant effect on the calculated mass recovery. Another other reason for failure to achieve total mass recovery has been attributed to long time scale storage and release over extended periods at concentrations below the detection limit of the fluorometer. The fact that this study achieved near total mass recovery may indicate that sediment storage in these rivers may in fact be only limited to the first few centimeters, a contention supported by the relatively low hydraulic conductivities

measured in the benthic sediments. This fraction of the sediments in which active exchange and storage is occurring is the hyporheic zone of these rivers.

Management Implications

From a management perspective, this study has several important implications in regards to the maintenance or restoration of submerged aquatic vegetation in spring-fed rivers. This study has shown that vegetation has strong effect on the mean velocity, and therefore the reach residence time. This study also showed that vegetation beds act as transient storage zones, which also increases the reach residence time. Nutrient loading, particularly in regards to nitrogen, has become a very important issue in these systems. In the last fifty years, many springs have seen nitrate concentrations increase by an order of magnitude over historic concentrations due to anthropogenic activities (Katz et al. 2001, Stevenson et al. 2007). Insofar as residence time is one of the major factors determining the magnitude of nutrient removal within a reach, it would appear that a high vegetation density should be a management target. Vegetation may have direct effects on nitrogen cycling (through assimilation), first-order indirect effects (by providing the carbon which drives denitrification) and second-order indirect effects by extending the residence time so that more assimilation and denitrification may occur.

As anthropogenic activities continue to increase nutrient loads of both surface and groundwater, the role of river systems as sinks for these nutrients has become ever more apparent. If we are to understand and predict the ecological implications of this increased loading both in the rivers themselves and their downstream receiving bodies, we must be able to accurately predict the transport properties and ultimate fates of nutrients in these systems. A prerequisite to developing an effective model of nutrient metabolism is to first determine the morphological and vegetative mechanisms which

control the solute transport properties of these systems. Spring-fed rivers are excellent model ecosystems because of their point-source nature and minimal lateral inputs, and understanding the mechanisms which control the hydraulic properties in these systems is an important early step in the ongoing process of determining these mechanisms in a more general sense for large rivers everywhere.

LIST OF REFERENCES

Akaike, H. 1974. A new look at the statistical model identification. IEEE Transactions on Automatic Control 19:716–723

Alexander, R.B., J.K. Bohlke, E.W. , M.B. David, J.W. Harvey, P.J. Mulholland, S.P. Seitzinger, C.R. Tobias , C. Tonitto, and W.M. Wollheim. 2009. Dynamic modeling of nitrogen losses in river networks unravels the coupled effects of hydrological and biogeochemical processes. Biogeochemistry 93:91–116.

Bencala, K.E., and R.A. Walters. 1983a. Simulation of solute transport in a mountain pool-and-riffle stream: a transient storage model. Water Resources Research 19:718–724.

Bencala, K.E., R.E. Rathbun, and A.P. Jackman. 1983b. Rhodamine WT dye losses in a mountain stream environment. Water Resources Bulletin. 19:943–950.

Bencala, K. E., V. C. Kennedy, G. W. Zellweger, A. P. Jackman, and R. J. Avanzino. 1984. Interactions of solutes and streambed sediment. An experimental analysis of cation and anion transport in a mountain stream. Water Resources Research 20:1797–1803.

Bencala, K.E., D.M. McKnight, and G.W. Zellweger 1990. Characterization of transport in an acidic and metal-rich mountain stream based on a lithium tracer injection and simulations of transient storage. Water Resources Research 26:989–100.

Carollo, F.G., V. Ferro, and D. Termini. 2002. Flow velocity measurements in vegetated channels. Journal of Hydraulic Engineering 128:644–673.

Carollo, F.G., V. Ferro, and D. Termini. 2005. Flow resistance law in channels with flexible submerged vegetation. Journal of Hydraulic Engineering 131:554–564.

Choi, J., J.W. Harvey, and M.H. Conklin. 2000. Characterizing multiple timescales of stream and storage zone interaction that affect solute fate and transport in streams. Water Resources Research 36:1511–1518.

Chow, V.T. 1959. Open-channel Hydraulics. McGraw-Hill, New York, New York, U.S.A.

Day, T.J. 1975. Longitudinal dispersion of natural streams. Water Resources Research 11:909–918.

Elder, J.W. 1959. The Dispersion of marked fluid in turbulent shear flow. Journal of Fluid Mechanics 5:544–560.

Ensign, S.H. and Doyle, M.W. 2006. Nutrient spiraling in streams and river networks. Journal of Geophysical Research 111:G04009.

Fischer, H.B. 1973. Longitudinal dispersion and turbulent mixing in an open channel. Annual Review of Fluid Mechanics 5:59–78.

Gooseff, M.N., S.M. Wondzell, R. Haggerty and J. Anderson. 2003. Comparing transient storage modeling and residence time distribution (RTD) analysis in geomorphically varied reaches in the Lookout Creek basin, Oregon, USA. Advances in Water Resources 26:925–937.

Harvey, J.W., B.J. Wagner and K.E. Bencala. 1996. Evaluating the reliability of the stream tracer approach to characterize stream-subsurface water exchange. Water Resources Research 32:2441–2451.

Hoyer, M.V., T.K. Frazer, S.K. Notestein and D.E. Canfield. 2004. Vegetative Characteristics of three low lying Florida coastal rivers in relation to flow, light, salinity and nutrients. Hydrobiologica 528:31–43

Jarvela, J. 2005. Effect of submerged flexible vegetation on flow structure and resistance. Journal of Hydrology 307:233–241.

Kadlec, R.H., and R.L. Knight. 1996. Treatment Wetlands. Lewis Publishers, Boca Raton, Florida, U.S.A.

Kouwen, N., T.E. Unny and H.M. Hill. 1969. Flow Retardance in Vegetated Channels. Journal of Irrigation and Drainage Engineering 95:329–344.

Kurtz, R.C., P. Sinphay, W.E. Hershfeld, A.B. Krebs, A.T. Peery, D.C. Woithe, S.K. Notestein, T.K. Frazer, J.A. Hale, and S.R. Keller. 2003. Mapping and monitoring of submerged aquatic vegetation in Ichetucknee and Manatee Springs. Suwannee River Water Management District, Live Oak, Florida, U.S.A.

Leopold, L.B., Maddock, T., 1953. The hydraulic geometry of stream channels and some physiographic implications. United States Geological Survey Professional Paper 52. U.S. Geological Survey, Washington D.C., U.S.A.

Leopold, L. B., M. G. Wolman, and J.P. Miller. 1964. Fluvial Process in Geomorphology. W. H. Freeman, New York, New York, U.S.A.

Lightbody A.F., and H.M. Nepf. 2006. Prediction of Velocity Profiles and Longitudinal Dispersion in Emergent Salt Marsh Vegetation. Limnology and Oceanography. 51:218–228.

Manning, R. 1890. On the flow of water in open channels and pipes. Transactions of the Institute of Civil Engineers of Ireland 20:161–207.

Manning, R. 1895. Supplement to on the flow of water in open channels and pipes. Transactions of the Institute of Civil Engineers of Ireland 24:179–207.

Murphy, E., M. Ghisalberti and H. Nepf. 2007. Model and laboratory study of dispersion in flows with submerged vegetation. Water Resources Research 43:W05438.

Nepf, H.M., C.G. Mugnier and R.A. Zavistoski. 1997. The Effects of Vegetation on longitudinal dispersion. Estuarine, Coastal and Shelf Science 44:675–684

Nepf, H.M. 1999. Drag, turbulence, and diffusion in flow through emergent vegetation. Water Resources Research 35:479-489.

Newbold, J.D., R.V. Oneill, J.W. Elwood and W. Van Winkle. 1982. Nutrient spiraling in streams: implications for nutrient limitations and invertebrate activity. The American Naturalist 120:628–652.

Odum, H.T. 1957a. Trophic structure and productivity of Silver Springs, Florida. Ecological Monographs 27:55–112.

Odum, H.T. 1957b. Primary production measurements in eleven Florida springs and a marine turtle-grass community. Limnology and Oceanography 2:85–97.

Palmer, V.J. 1945. A method for designing vegetated waterways. Agricultural Engineering 26:516–520.

Park, C.C. 1977. World wide variations in hydraulic geometry exponents of stream channels: an analysis and some observations. Journal of Hydrology 33:133–146.

Ree, W.O. 1949. Hydraulic characteristics of vegetation for vegetative waterways. Agricultural Engineering 30:184–189.

Runkel, R.L. 1998. One-dimensional transport with inflow and storage (OTIS): a solute transport model for streams and rivers. USGS Water-Resources Investigations Report 98–4018. U.S. Geological Survey, Denver, Colorado, U.S.A.

Runkel, R.L. 2007. Toward a transport-based analysis of nutrient spiraling and uptake in streams. Limnology and Oceanography 5:50–62.

Sabatini, D.A. and T.A. Austin, 1991. Characteristics of rhodamine WT and fluorescein as adsorbing ground-water tracers. Ground Water 29:341–349.

Sand-Jensen, K., and J. Mebus. 1996. Fine-scale patterns of water velocity within macrophyte patches in streams. Oikos 76:169–180.

Seitzinger, S.P., R.V. Styles, E.W. Boyer, R.B. Alexander, G. Billen, R.W. Howarth, B. Mayer and N. Van Breemer. 2002. Nitrogen retention in rivers: model development and application to watersheds in the northeastern U.S.A. Biogeochemistry 57:199–237.

Shucksmith, J.D, J.B. Boxall and I. Guymer. 2010. Effects of emergent and submerged natural vegetation on longitudinal mixing in open channel flow. Water Resources Research 46:W04504.

Scott, T., G. Means, R. Meegan, R. Means, S. Upchirch, R. Copeland, J. Jones, T. Roberts and A. Willet. 2004. Springs of Florida. Bulletin No.66, Florida Geologic Survey, Tallahassee, Florida, U.S.A.

Smart, P.L. and I.M.S. Laidlaw.1977. An evaluation of some fluorescent dyes for water tracing. Water Resources Research 13:15–33.

Stream Solute Workshop (S.S.W.). 1990. Concepts and methods for assessing solute dynamics in stream ecosystems. Journal of the North American Benthological Society 9:95–119.

Tank, J.L., E.J. Rosi-Marshall, M.A. Baker and R.O. Hall. 2008. Are rivers just big streams? A pulse method to quantify nitrogen demand in a large river. Ecology 89:2935–2945.

Taylor, G.I. 1954. Dispersion of soluble matter in solvent flowing slowly through a tube. Proceedings of the Royal Society of London 223:446–468.

Vitousek, P.M, J.D. Aber, R.W. Howarth, G.E. Likens, P.A. Matson, D.W. Schindler, W.H. Schlesinger and D.G. Tilman. 1997. Human Alterations of the Global Nitrogen Cycle. Ecological Applications 7:737–750.

Wilson, C.A.M.E. and M.S. Horritt. 2002. Measuring the flow resistance of submerged grass. Hydrological Processes 16:2589–2598.

Wilson, C.A.M.E., T. Stoesser, P.D. Bates and A. Batemann Pinzen. 2003. Open channel flow through different forms of submerged flexible vegetation. Journal of Hydraulic Engineering. 129:847–853.

Wilson, C.A.M.E. 2007. Flow resistance models for flexible submerged vegetation. Journal of Hydrology 342:213–222.

BIOGRAPHICAL SKETCH

Robert Hensley received his bachelor's degree in environmental engineering from the University of Florida in 2006. He then worked for Watershed Concepts, a consulting engineering firm in Jacksonville, Florida, performing hydrologic modeling and floodplain mapping. He returned to the University of Florida in 2008 and completed his master's degree in 2010. He plans to remain at the University of Florida and pursue a Ph.D. in the interdisciplinary ecology program.